

1-1-2013

Impedance Estimation Using Randomized Pulse Width Modulation and Power Converters

William M. McCoy
University of South Carolina

Follow this and additional works at: <https://scholarcommons.sc.edu/etd>



Part of the [Electrical and Electronics Commons](#)

Recommended Citation

McCoy, W. M.(2013). *Impedance Estimation Using Randomized Pulse Width Modulation and Power Converters*. (Master's thesis). Retrieved from <https://scholarcommons.sc.edu/etd/2411>

This Open Access Thesis is brought to you by Scholar Commons. It has been accepted for inclusion in Theses and Dissertations by an authorized administrator of Scholar Commons. For more information, please contact digres@mailbox.sc.edu.

IMPEDANCE ESTIMATION USING RANDOMIZED PULSE WIDTH MODULATION
AND POWER CONVERTERS

by

Matthew McCoy

Bachelors of Science
University of South Carolina, 2013

Submitted in Partial Fulfillment of the Requirements

For the Degree of Masters of Science in

Electrical Engineering

College of Engineering and Computing

University of South Carolina

2013

Accepted by:

Herbert Ginn III, Major Professor

Roger Dougal, Committee Member

Lacy Ford, Vice Provost and Dean of Graduate Studies

© Copyright by Matthew McCoy, 2013
All Rights Reserved.

ACKNOWLEDGEMENTS

I would like to thank my advisor Dr. Herbert Ginn III for his leadership throughout my graduate studies. I also appreciate the efforts of my committee member Dr. Roger Dougal, as well as the rest of my graduate and undergraduate professors. Special thanks are also extended to my friends, family, and David Metts for their support throughout my studies.

ABSTRACT

With the adoption of technologies such as alternative energy production, DC power grids, and electric vehicles, the use of high power switching converters has seen a dramatic increase. These power converters serve many rolls such as grid-tied inverters in solar farms, high power charging for electric vehicles, motor drives for industrial applications, and DC links in transmission systems. With the increased prevalence of such devices, it is only natural to attempt to optimize their operation. As with any level of converter, it is desirable to have accurate control over the generated voltages and currents. Often, these controllers implement some form of predictive control which requires knowledge of system parameter values to operate properly. Due to several factors, including temperature and component non-linearity, these component values can vary during normal operation. This can lead to degradation of closed loop control and system instabilities. If one is able to measure system parameters while the converter is operating, control parameters can be updated in real time to optimize the system performance.

A significant percentage of the size and cost of switching converters are filter elements meant to reduce the amount of noise injected into other attached circuits, or in the case of grid-tied converters, noise injected into the grid. As power levels increase, the size, cost, and power lost in the filter becomes greater. To minimize these negative effects, methods have been developed that reduce harmonic injections, thus allowing for

smaller filter elements. One such technique is Randomized Pulse Width Modulation which removes the large harmonic spikes present in standard switching systems, and replaces them with a wide frequency energy spectrum.

The objective of this research is to examine the feasibility of online impedance identification by combining and modifying existing technologies. Specifically, Randomized Pulse Width Modulation and Wideband System Identification techniques are used to simultaneously reduce system noise and create an estimation of system filter element impedances. This allows for the reduction of the filter size while simultaneously providing a real-time estimate of the filter impedance with the goal of better feedback control performance.

TABLE OF CONTENTS

ACKNOWLEDGEMENTS.....	iii
ABSTRACT	iv
LIST OF TABLES	viii
LIST OF FIGURES	ix
LIST OF ABBREVIATIONS.....	xii
CHAPTER 1 INTRODUCTION.....	1
CHAPTER 2 PULSE WIDTH MODULATION.....	6
2.1 Deterministic Pulse Width Modulation	6
2.2 Randomized Pulse Width Modulation.....	9
CHAPTER 3 SYSTEM IDENTIFICATION.....	14
3.1 Previous Methods for Identification	14
3.2 RPWM for System Identification	21
CHAPTER 4 IMPLEMENTATION	24
4.1 Identification Routine	25
4.2 Measured Impedance Averaging	27
4.3 Least Squares Fitting.....	27

4.4 Buck Converter	28
4.5 Single Phase Grid-Tied Converter	41
CHAPTER 5 HARDWARE VALIDATION	47
CHAPTER 6 PRACTICAL CONSIDERATIONS FOR IDENTIFICATION	53
6.1 Sampling Time and Frequency	53
6.2 Sampling Resolution	55
CHAPTER 7 CONCLUSION AND FUTURE WORK	58
REFERENCES	61
APPENDIX A – RPWMII MATLAB S-FUNCTION	63
APPENDIX B – FFT AVERAGING MATLAB	69
APPENDIX C – LEAST SQUARES MATLAB FUNCTION	72

LIST OF TABLES

Table 4.1 Simulation Values for DPWM Buck Converter	32
Table 4.2 Simulation Results for Inductance Calculation	40
Table 4.3 Simulation Values for DPWM Grid-Tied Inverter	43
Table 4.4 Improvements Using Least Squares Fitting	45
Table 5.1 Actual Component Values for Buck Converter	47
Table 5.2 Calculated Inductance Values	52
Table 6.1 Execution Comparison Between Fourier Transform and FFT	53

LIST OF FIGURES

Figure 1.1 Half Bridge Voltage Source Converter	2
Figure 2.1 Carrier Based Pulse Width Modulation comparison	7
Figure 2.2 Corresponding CPWM gate signals	7
Figure 2.3 Buck converter input current frequency spectrum	8
Figure 2.4 Randomized switching frequency carrier based PWM	10
Figure 2.5 Sampling time switching time relationship	10
Figure 2.6 RPWMII timing scheme.....	12
Figure 2.7 RPWMII versus DPWM current spectrum.....	12
Figure 3.1 Switching states of PRBS versus DPWM	19
Figure 3.2 DPWM current frequency spectrum.....	20
Figure 3.3 PRBS current frequency spectrum	20
Figure 3.4 RPWMII current frequency spectrum	22
Figure 4.1 General methodology for impedance calculation.....	26
Figure 4.2 Buck converter with ideal switches	29
Figure 4.3 Square wave with harmonics	30
Figure 4.4 Buck converter used for simulation.....	31

Figure 4.5 Current frequency spectrum of DPRM buck converter simulation.....	33
Figure 4.6 RPWMII current frequency spectrum	34
Figure 4.7 Expected Bode plot for $Z(j\omega)$	35
Figure 4.8 Constructed impedance using RPWMII.....	36
Figure 4.9 Constructed impedance using RPWMII and averaging	37
Figure 4.10 Constructed RL impedance using RPWMII and averaging	38
Figure 4.11 Constructed RL impedance using RPWMII and averaging ZOOM	39
Figure 4.12 Single phase, grid-tied converter.....	41
Figure 4.13 Grid-tied converter simulation	42
Figure 4.14 DPWM inverter simulated current frequency spectrum.....	43
Figure 4.15 RPRMII inverter simulated current frequency spectrum	44
Figure 4.16 RPWMII Inverter impedance reconstruction ZOOM.....	45
Figure 5.1 Current sensor schematic.....	48
Figure 5.2 Hardware validation $C = 470\mu\text{F}$	49
Figure 5.3 Hardware validation $C=800\mu\text{f}$	49
Figure 5.4 Measured current frequency spectrum	50
Figure 5.5 Impedance reconstruction with $L=330\mu\text{H}$	51
Figure 5.6 Impedance reconstruction with $L=660\mu\text{H}$	51
Figure 6.1 Importance of frequency resolution.....	55

Figure 6.2 Importance of ADC resolution to identification.....	56
Figure 6.3 Typical ADC frequency characteristics (TI ADS7863)	57

LIST OF ABBREVIATIONS

PWM.....	Pulse Width Modulation
DPWM	Deterministic Pulse Width Modulation
RPWM	Randomized Pulse Width Modulation
CBPWM.....	Carrier Based Pulse Width Modulation
VSC.....	Voltage Source Converter
DFT	Discrete Fourier Transform
ESR	Equivalent Series Resistance
MOSFET.....	Metal Oxide Semiconductor Field Effect Transistor
IGBT	Insulated Gate Bipolar Transistor

CHAPTER 1

INTRODUCTION

Modern switching converters provide many advantages over the previous technologies they are replacing. DC to DC switching converters provide higher efficiencies than older linear regulators, which can lead to an increase in battery life for mobile devices. Active rectifiers outperform simple rectification by allowing for controlled power factor, nearly sinusoidal current draw, and reduced noise injected into the AC source. [1] These advantages come at the cost of more complex closed loop controllers. Whereas linear voltage regulators can easily be implemented with simple passive and active components, a switching regulator often necessitates the use of a higher level controller such as a microcontroller or dedicated control circuit. Similarly, while rectification can be accomplished with diodes and capacitors, active rectifiers require the use of switching elements, feedback sensors, as well as controllers. This has spurred the ongoing development of new and improved control algorithms meant to optimize factors such as efficiency, cost, and system reliability. [2] With any power converters, it is desirable to maintain a minimum level of closed loop control performance at all times. If control is lost, negative consequences such as unstable regulation, large transients, and hardware damage can occur. Generally, the effectiveness of the controller is determined by the accuracy of the mathematical model of the system used when designing the control parameters. These models can range from the simple to the complex, and have proven to be a large field of study. [3] [4]

One of the most prevalent types of power electronic converter is the Voltage Source Converter. This converter's popularity arises from the fact that depending on the controls used, it can perform several different applications. In its simplest form, the half bridge VSC, the system is composed of two switching elements, a filter, a split bus, and a load. (Figure 1.1) It is important to note that this load can represent several things depending on the application. If this topology were to be used as a motor controller the load would represent the current draw of the motor as well as the back electromotive force. Here, a grid-tied converter is shown where the “load” is represented by a sinusoidal voltage source.

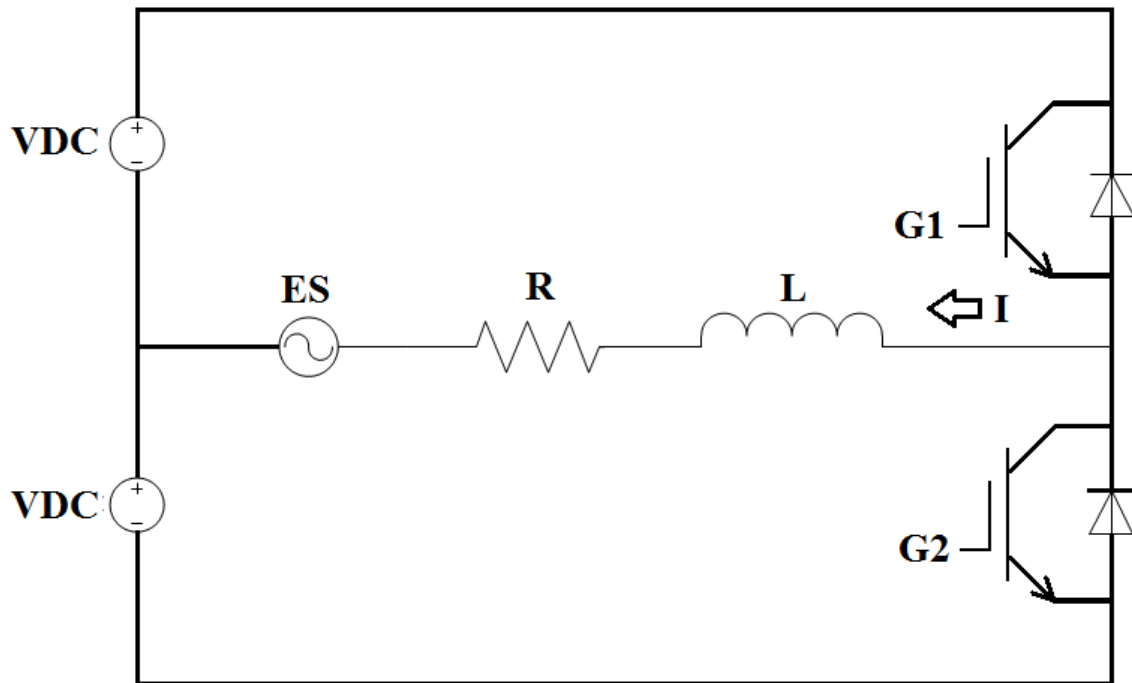


Figure 1.1 Half Bridge Voltage Source Converter

When the current flowing through the branch is considered the output of the system, the circuit can be represented in the state space form as follows.

$$\begin{aligned}\hat{x} &= Ax + Bu \\ y &= Cx + Du\end{aligned}$$

where

$$x = [I] \quad u = [2VDC, ES]^T \quad y = [I]$$

$$A = \begin{bmatrix} -R/L \end{bmatrix} \quad B = \begin{bmatrix} 1/L, -1/L \end{bmatrix} \quad C = [1] \quad D = [0, 0]$$

The transfer function between the converter voltage and current can then be found through use of the Laplace transform. (1)

$$G_{iv}(s) = \frac{1}{R + sL} \tag{1}$$

As can be seen, the converter dynamics rely heavily on the parameter impedance values. If these impedance values change during operation, the power converter can suffer from performance degradation. In particular, the filter inductance is known to be a component whose value can drift due to temperature, core material, and other operating conditions. Previous work has shown that this changing inductance can have a detrimental effect on the performance of such converts. [5] For this reason, it is desirable to have a means of measuring such impedance values. Classical tools such as network analyzers and dedicated inductance-capacitance-resistance meters perform an adequate job but suffer from the fact that they are unable to make measurements while the converters are in operation. This means that potential impedance values that change during certain operating conditions could be overlooked. Ideally, one would measure the impedance during operation to ensure that all of the characteristics are captured and properly accounted for. This information can then be used to update controller values to provide better performance over a range of operating conditions.

Previous research has already shown the feasibility of using a system's switching and sensing to affectively accomplish system identification. [6] [7] [8] These methods rely on the ability of the converter to act as a network analyzer by injecting test sequences into the system and measuring the response. This allows for the measurement of such characteristics as voltage and current gain, as well as impedances of passive components. While these techniques have proven to perform the job of system identification admirably, they do require the injection of previously nonexistent perturbations into the system, either through an intentional transient or some form of dithering. These perturbations are minimized to ensure that control outputs are maintained within acceptable limits while still exciting the system enough to make an accurate measurement. For example, in a DC-DC converter the perturbations could increase the output voltage ripple and inductor current ripple. Therefore, a tradeoff is made between the amplitude of perturbation (related to the potential accuracy of identification) and acceptable limits of output variation.

Beyond potentially increasing output ripple, these existing methods still have some of the drawbacks of standard converters. One such drawback is the switching harmonics present in most switching converters. [9] Switching harmonics are caused by the fixed switching frequency and can lead to large currents at the switching frequency and its harmonics. These harmonics are detrimental to the overall power quality and their mitigation is of paramount importance. Traditional methods of filtering such as low pass filters are affective, but for high power applications losses through these components and component cost become significant. Alternatively, it has been shown that these harmonics can be attenuated through careful control of converter switching signals. [9]

Essentially, by constantly varying the switching frequency, one can remove large harmonic spikes and replace them with a wider band, flat noise spectrum. The objective of this work is to use this flat frequency band injection as the test signal, while using existing methods of identification to accurately measure system impedances for power converters. This will achieve the goal of near-real-time impedance measurements, while also having the advantage of minimized switching harmonics.

CHAPTER 2

PULSE WIDTH MODULATION

Voltage source converters accomplish their control action through the use of precisely timed switching signals. These switching states are determined by sampling system outputs, and through means of a digital controller, calculating the necessary switch mode. Methods of switching fall into two general categories, deterministic and randomized. In the deterministic scheme, switching and sampling times are kept constant based on a designed switching and sampling frequency. Randomized switching varies the switching time, and possibly the sampling time, on a cycle-to-cycle basis. This chapter will present three separate sub categories of modulation and examine how they affect the operation of the system.

2.1 Deterministic Pulse Width Modulation

While there have been numerous forms of Deterministic Pulse Width Modulation developed, each with its own advantages, they all share the common characteristic of a set switching frequency. One of the simplest forms of DPWM is Carrier-Based Pulse Width Modulation. With CBPWM, a triangular carrier wave is created and compared to the controller's generated reference signal. The switch states are then determined by results of the comparison of the two waves. Here, a low frequency sinusoidal reference is being compared to a much higher frequency carrier wave (Figure 2.1) which generates the corresponding gate signals. (Figure 2.2).

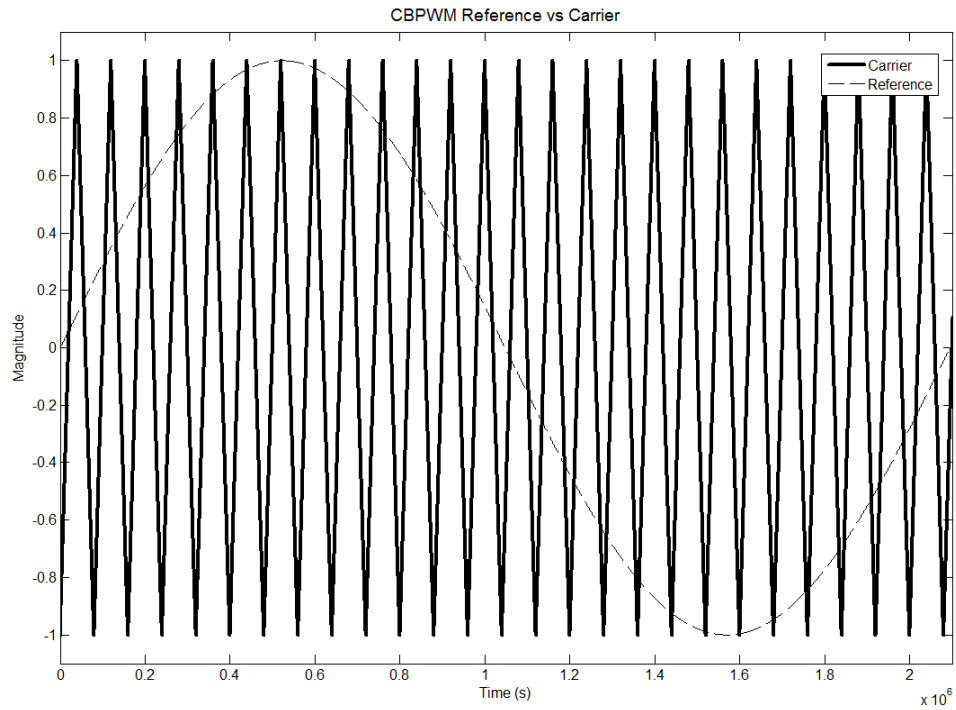


Figure 2.1 Carrier Based Pulse Width Modulation comparison

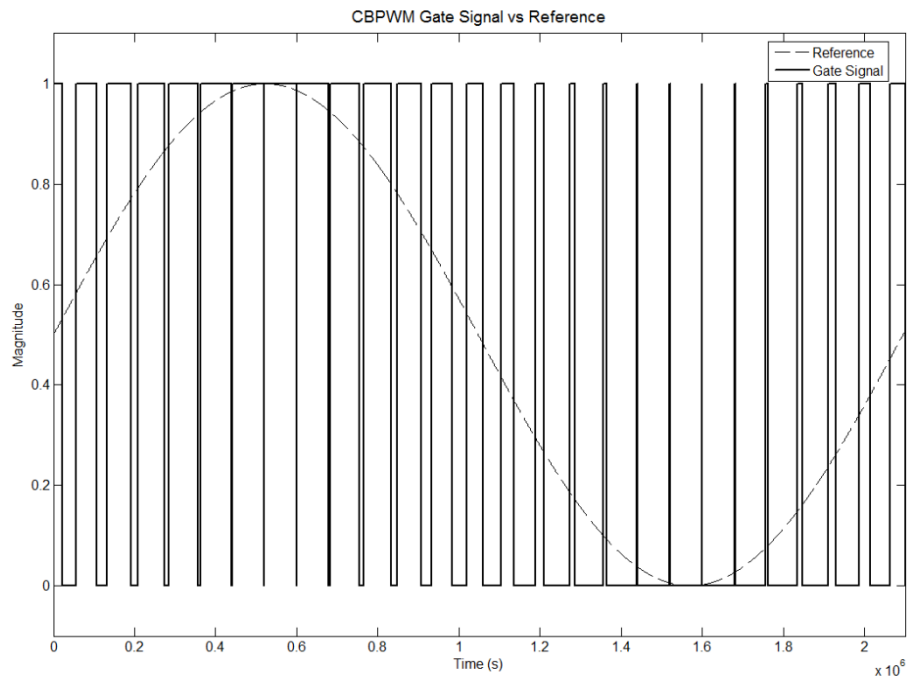


Figure 2.2 Corresponding CPWM gate signals

Several factors go into the selection of a controller's switching frequency. These factors include, processor speed, system bandwidth, switch characteristics, and filter type. It is desirable that the switching not add any disturbances to the system, so in practice low pass filters are used to mitigate switching noise. The design engineer is tasked with selecting a filter that will minimize noise while also considering factors such as filter size, cost, complexity, and power loss. These compromises mean that the switching noise can never be completely eliminated. Not only will noise be introduced at the switching frequency, but also at harmonic orders of the switching frequency. In grid tied applications this can decrease power quality, increase transformer heating, create acoustic noise, and be potentially damaging to other equipment. [9] In the example of a Buck converter using DPWM, these harmonics can easily be seen when viewing the frequency spectrum of the system input current. (Figure 2.3)

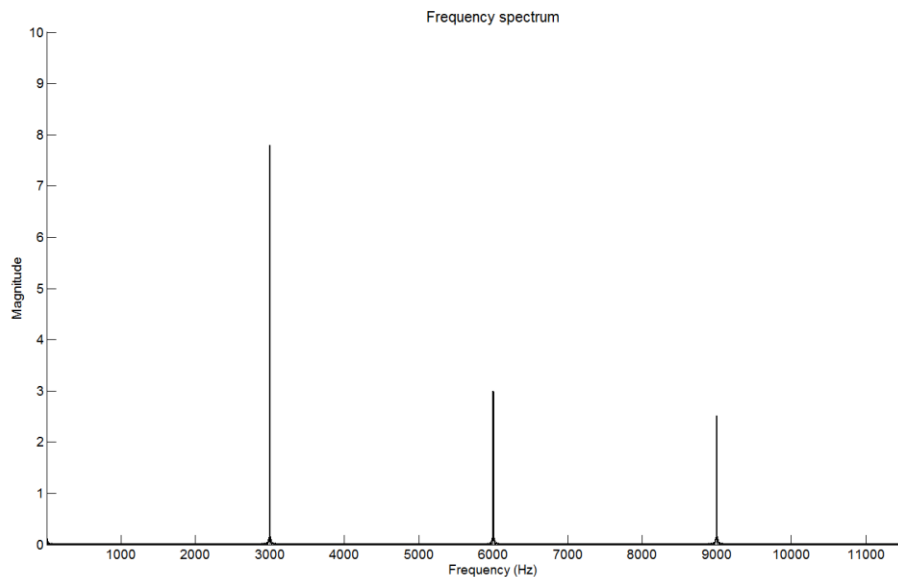


Figure 2.3 Buck converter input current frequency spectrum

It is not always feasible to reduce switching noise by increasing filter performance as there may be design limits on the filter elements. For this reason, it is desirable to minimize these harmonics through means other than simple passive filtering. One such solution is the use of Randomized Pulse Width Modulation.

2.2 Randomized Pulse Width Modulation

In an attempt to mitigate injected switching noise without the use of extra filtering, techniques for Randomized Pulse Width Modulation have been developed. At the core of RPWM is the concept of a constantly varying switching frequency over a predetermined frequency range. The goal of RPWM is to eliminate the characteristic harmonic spikes cause by DPWM, and replace them with a wide band of noise. While there is still noise being injected, spreading it across a frequency band is advantageous to the elimination of acoustic noise, possible grid damage, and power quality issues. [9]

2.2.1 Randomized Carrier Frequency PWM

One method of RPWM is the use of a randomly varying switching frequency. With deterministic CBPWM, the frequency of the carrier wave is held constant, leading to the aforementioned harmonic current spikes. In contrast, randomized carrier based PWM is achieved by changing the slope of the carrier wave on a cycle by cycle basis. As CBPWM switching frequency is based upon the intersection of the carrier wave and the reference wave, increasing the carrier wave slope increases the switching frequency while decreasing the slope decreases the switching frequency. (Figure 2.4)

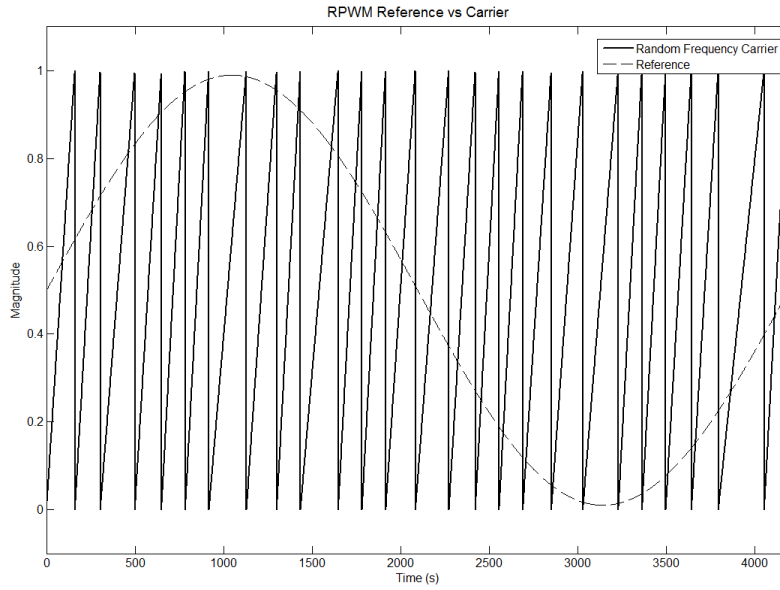


Figure 2.4 Randomized switching frequency carrier based PWM

While this method of RPWM achieves the desired goal of modulating the switching frequency, it does have drawbacks when implemented in an actual system. One of the main concerns with this type of implementation is the connection between switching frequency and sampling frequency. (Figure 2.5)

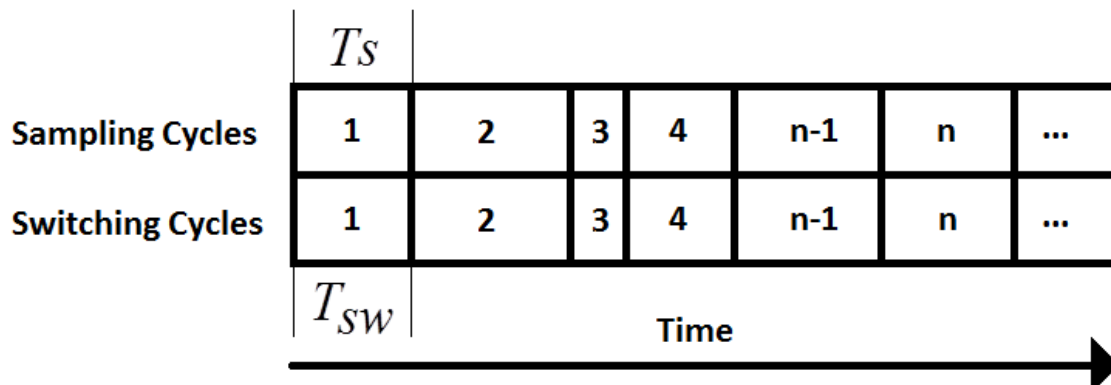


Figure 2.5 Sampling time switching time relationship

As can be seen, the sampling time is no longer constant; rather, it is constantly changing in synchronization with the randomized switching frequency. This makes the implementation of a digital controller very difficult as the sampling time step is used in the calculation of future outputs. This also limits the minimum switching time (maximum switching frequency) to the time necessary for a control iteration. Ultimately, this means the maximum switching frequency is limited by factors such as ADC sampling times, control algorithm execution times, and any other controller overhead. For these reasons, it is beneficial to use a system of RPWM that decouples the switching frequency from the system sampling time.

2.2.2 RPWM II

A system of randomized pulse width modulation has been developed that provides the advantages of RPWM (minimized harmonic injections), while having the added benefit of a fixed sample time. [9] This method, here called RPWMII, uses a fixed sampling frequency and a randomly generated time delay between the start of subsequent switching cycles. This time delay, denoted Δt , is calculated by (2) where r is a random number varying over the range 0 to 1, and τ is the sampling period.

$$\Delta t = \tau * r \quad (2)$$

Care must be taken when calculating values of Δt as they could inadvertently exceed the limitations of the system. To avoid possible collisions, the switching period is limited to values between T_{min} and 2τ . The limit T_{min} ensures that any operations of the controller (sampling, communications, calculations, etc.) can be completed before the next switching cycle. (Figure 2.6)

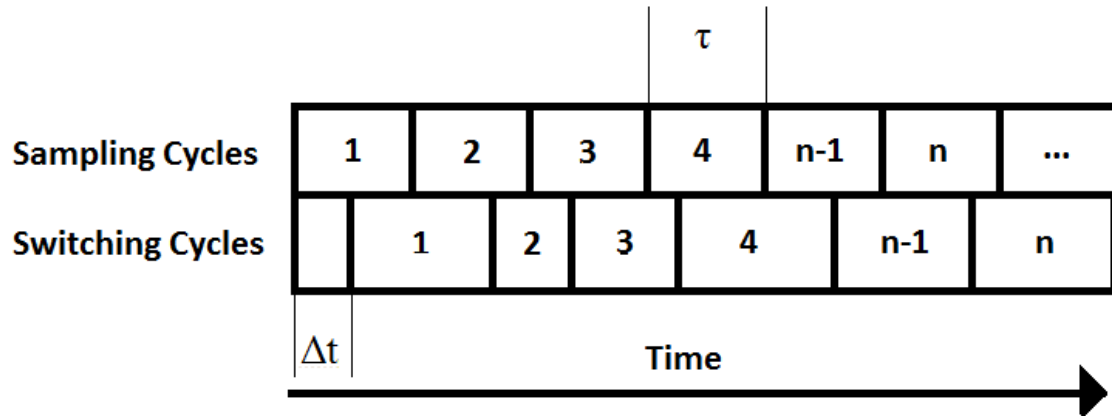


Figure 2.6 RPWMII timing scheme

The RPWMII algorithm [10] is simulated in MATLAB and Simulink to determine the effectiveness of harmonic mitigation. (Figure 2.7) When compared to the same circuit using DPWM switching at 6kHz, it can easily be seen that the characteristic harmonic spikes have been eliminated and replaced with a wide distribution in the frequency spectrum.

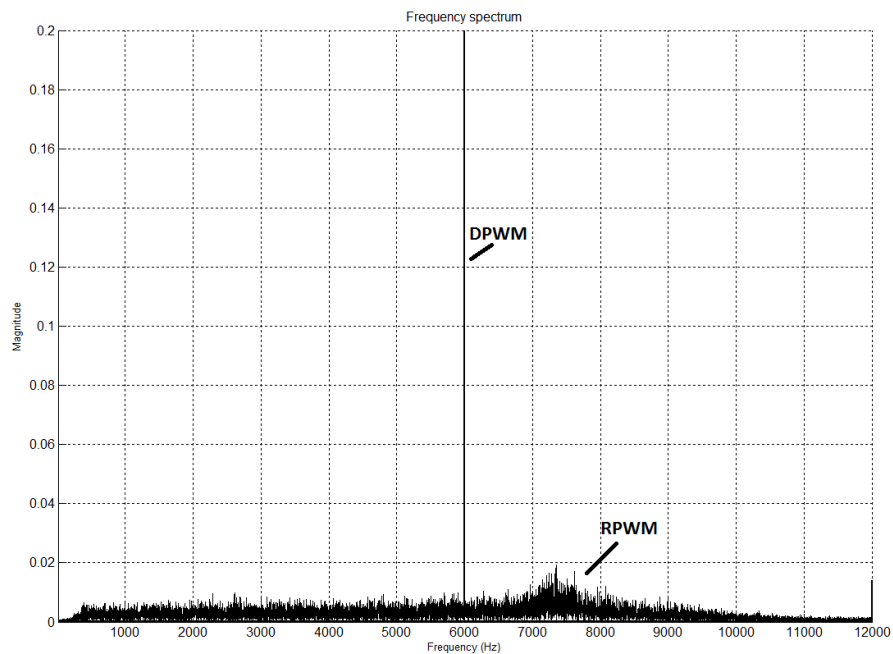


Figure 2.7 RPWMII versus DPWM current spectrum

Not only does RPWMII serve to minimize the harmonic current spikes, but it has the added benefit of injecting a wide-bandwidth sequence into the system. The next chapter will discuss how this sequence can be used to perform system identification within switching converters.

CHAPTER 3

SYSTEM IDENTIFICATION

There are several existing methods of identification designed for a multitude of different systems. These approaches are used to model several types of systems ranging from the dynamics of an industrial process to the steering controls of large ships and more importantly the open-loop characteristics of switching converters. [11] The general concept of each type of system identification is to measure inputs and outputs, then through some method, develop a mathematical model of the system in question. With a model in hand, a control scheme can be created, or in the case of on-line identification, an existing controller can be honed to improve performance.

3.1 Previous Methods of Identification

With so many possible methods of identification available, it is necessary to determine the proper technique for the given situation. Considerations must be made regarding desired accuracy, measurements available, type of system under test, and physical limitations of the measurement equipment. All of these methods take advantage of the fact that switching converters already have sensors in place to measure necessary voltages and currents. This essentially allows the switching converter to measure its own characteristics without the need for any extra equipment.

3.1.1 Step Response

One of the simplest methods for identification of an unknown system is the step response technique. This type of identification is commonly used for the modeling of industrial processes such as material level controls, heating and cooling, and speed controllers. [12] [13] For a first-order, linear system, the process attempts to approximate the necessary gain, K , and time constant, T , to match with a first-order model (3).

$$Y(s) = \frac{K}{Ts + 1} U(s) \quad (3)$$

As can be seen in the above equation, the system input, $U(s)$, and output, $Y(s)$, can be used to calculate the desired model parameters. During the identification, the input is carefully given a step change while the output is closely monitored. These are the values then used to construct the simple system model. While this is an effective and often used method for system identification, it does have disadvantages. The need for a step change requires that the output be altered by some non-negligible amount. This may be acceptable if the system is offline or if the step size can be minimized, but often the step needs to be relatively large to rise above the noise present in the system. If this were to be used for a grid tied converter, it would be necessary to ensure that the grid could handle the transients introduced. Also, the difficulty in model matching increases with the order of the system to the point where complex non-linear systems may not be able to be identified.

3.1.2 Cross-Correlation Methods

Another common way to perform system identification within power converters is the Cross-Correlation Technique. As opposed to the step response method, the cross-

correlation system does not require any large transients to excite the device under test. Instead, a wide-bandwidth test sequence is injected into the switching converter control signal and the voltages and currents are measured to determine the desired system parameters. [6] [7] [8] This method has been shown to be very effective in determining things such as the control-to-output transfer function as well as system impedances.

At the core of this technique is the ability to inject a suitable test sequence into the control of the converter under test. A sampled switching converter operating in steady state can be described by (4)

$$y[n] = \sum_{k=1}^{\infty} h[k]u[n-k] + v[n] \quad (4)$$

Here, $y[n]$ is the sampled output, $h[n]$ is the discrete-time system impulse response. $u[n]$ is the sampled input, and $v[n]$ is any noise in the system. In a switching converter, the input represents the PWM control signal and the output can be measured voltages or currents. When the cross correlation of the input and output is taken, (4) becomes (5).

$$R_{uy}[n] = \sum_{n=1}^{\infty} h[n]R_{uu}[m-n] + R_{uv}[m] \quad (5)$$

If we assume the input signal to be white noise to meet the aforementioned requirement of a wide-bandwidth injection, assumptions can be made regarding the parameters in (5). For true white noise, an equal frequency spectrum over an infinite band of frequencies, the following holds true for the autocorrelation of the input (6) and the cross-correlation of the input to disturbances. (7)

$$R_{uu}[m] = \delta[m] \quad (6)$$

$$R_{uv}[m] = 0 \quad (7)$$

Here, $\delta[m]$ represents the system discrete impulse signal and when put into (5) leads to the simplified equation for input-to-output cross-correlation. (8) If the discrete Fourier transform (DFT) is then taken, the result is the input-to-output transfer function.

(9)

$$R_{uy}[m] = h[m] \quad (8)$$

$$G_{uy}[e^{j\omega}] = \text{DFT}\{h[m]\} \quad (9)$$

As the sensed outputs of most power converters are voltage and current, two distinct transfer functions can be found: control-to-voltage $G_{vd}[e^{j\omega}]$ and control-to-current $G_{id}[e^{j\omega}]$. If impedance measurement is the goal, Ohm's law can be used as such.

(10)

$$\frac{G_{vd}[e^{j\omega}]}{G_{id}[e^{j\omega}]} = \frac{\frac{\hat{v}[e^{j\omega}]}{\hat{d}[e^{j\omega}]}}{\frac{\hat{i}[e^{j\omega}]}{\hat{d}[e^{j\omega}]}} = \frac{\hat{v}[e^{j\omega}]}{\hat{i}[e^{j\omega}]} = Z[e^{j\omega}] \quad (10)$$

This can be further simplified to show that for impedance measurements, it is only necessary to take the ratio of the DFT of the measured voltage and current. (11)

$$\frac{\text{DFT}\{v[n]\}}{\text{DFT}\{i[n]\}} = Z[e^{j\omega}] \quad (11)$$

Previously, an assumption was made that the input test sequence could be approximated as pure white noise. While examination of this assumption is outside the scope of this paper, some general observations can be made. Firstly, in previous work the test sequence utilized the superposition of a pseudo-random binary sequence (PRBS) upon the system control signal. This effectively dithers the PWM over a set range of frequencies. The upper limit of this injected frequency is limited to $F_{samp}/2$ by the Nyquist criterion, where F_{samp} is the system sampling frequency. The lower frequency limit and frequency resolution is determined by the PRBS length. In general, a tradeoff of a higher frequency band can be achieved at the cost of increased computational requirements such as time and memory. The literature has shown that this is an effective means of system identification, particularly with the measurement of impedances, though it does still have its limitations.

The PRBS injection works by either adding or subtracting some small amount of time to the switching cycles, on a cycle by cycle basis. This means that the switching frequency only has two effective states during an active injection. (Figure 3.1)

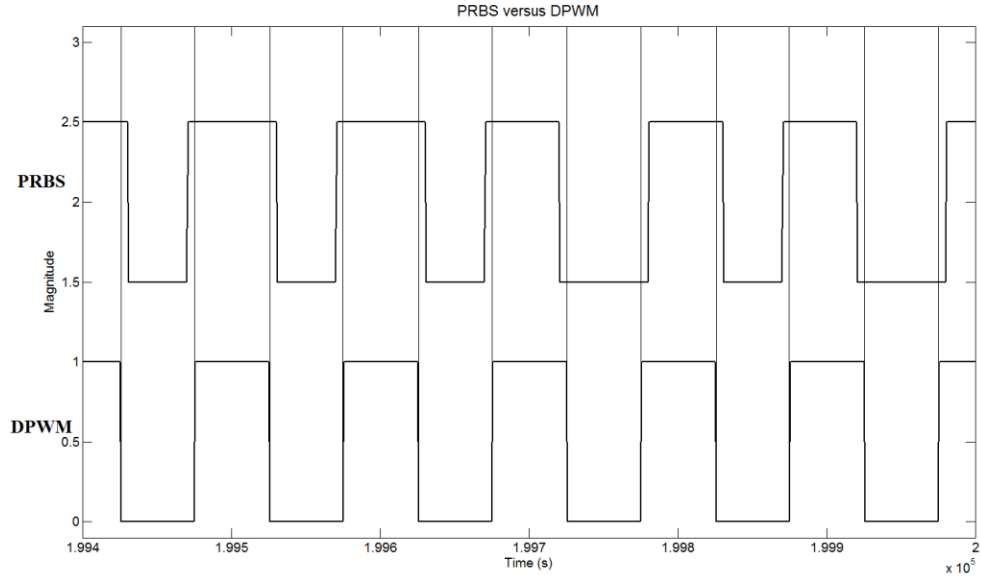


Figure 3.1 Switching states of PRBS versus DPWM

Because there are only two possible switching frequencies during an injection, large harmonic spikes are still present as in standard DPWM switching. When the frequency spectrum of a converter using DPWM (Figure 3.2) and one undergoing a PRBS injection (Figure 3.3) are compared, they look very similar. Both have the characteristic spikes at the switching frequency and its harmonics, while the PRBS spectrum has additional wide frequency components down towards DC.

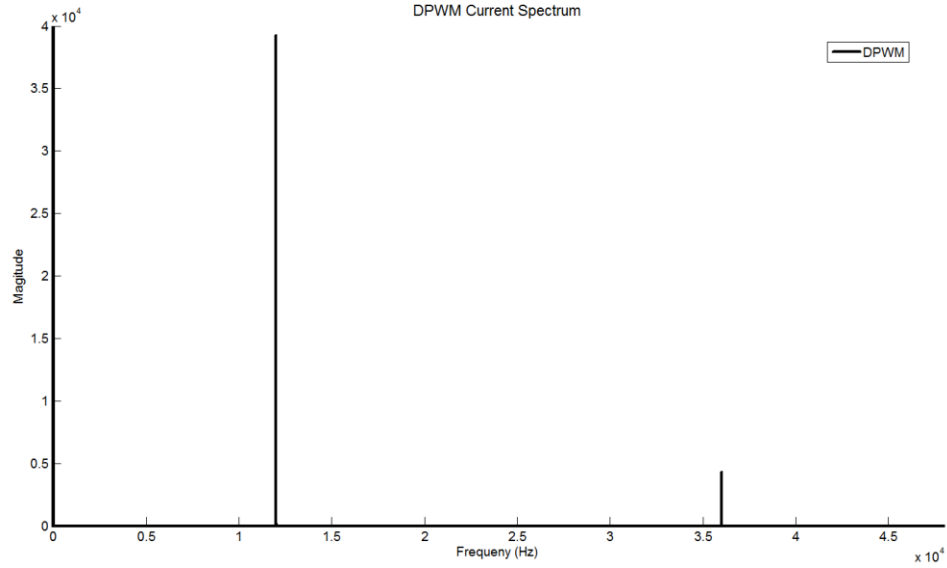


Figure 3.2 DPWM current frequency spectrum

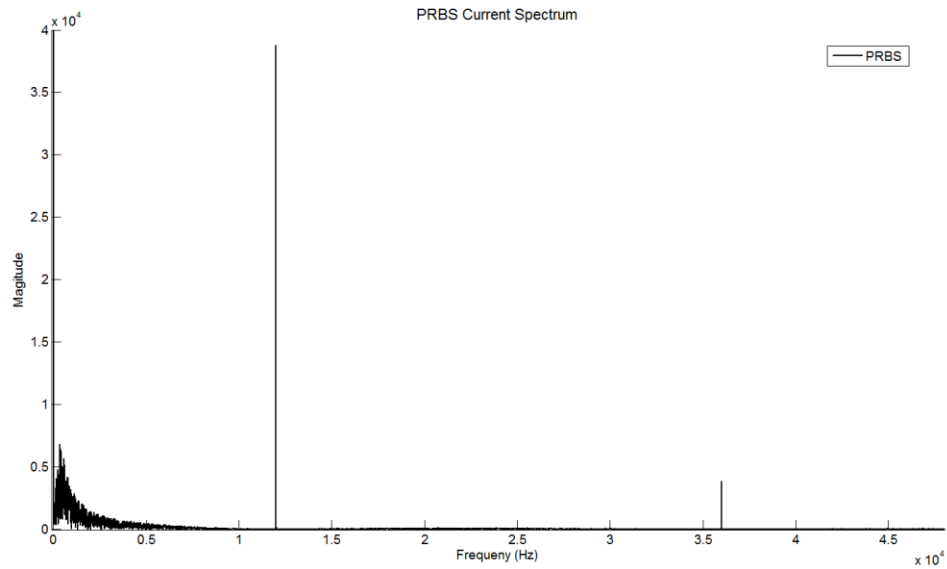


Figure 3.3 PRBS current frequency spectrum

For this reason, this identification method will be modified to use RPWMII as the source of frequency injections. This allows for the identification without the need for

extra equipment (sensors) while simultaneously providing the advantages of reduced harmonic injections.

3.2 RPWM for System Identification

System identification using RPWM has two distinct advantages. First, as will be shown, it does an adequate job of identifying system impedances within the range of injected frequencies. Secondly, as was shown in Figure 2.7, harmonic current spikes of switching converters can be greatly reduced without the need for extra filtering components. As opposed to the other methods described at the beginning of Chapter 3 that require the deliberate injection of some type of test sequence, RPWMII is constantly injecting frequency information into the system. This also means that there will be no difference in outputs, be it voltage or current, between the identification state and normal operation.

As discussed in section 2.2.2, there are natural limits to the range of injected switching frequencies. The aforementioned T_{min} and 2τ correspond to the maximum injected frequency and minimum injected frequency respectively. Because the limits on possible switching frequencies are determined by the RPWMII algorithm, they will be held constant throughout experimentation. As long as the method of randomization within the RPWMII algorithm is truly random, the injected frequencies are evenly distributed over the defined range of frequencies. The frequency spectrum of a switching converter utilizing RPWMII clearly shows a “bleeding” of the spectral information down into the sub switching frequencies. (Figure 3.4) These frequencies correspond to the range over which system information is desired.

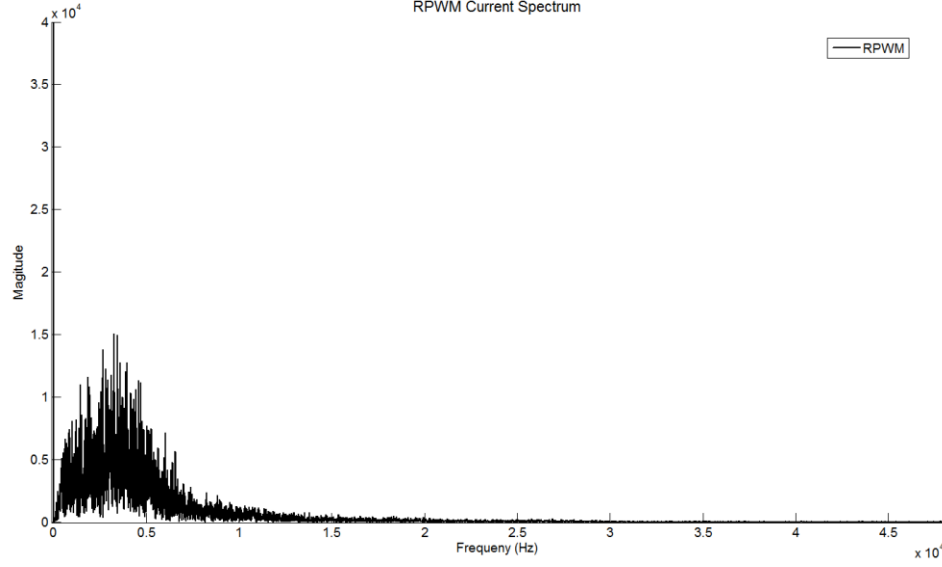


Figure 3.4 RPWMII current frequency spectrum

These injected frequencies serve as an analog to the PRBS injection in the cross-correlation technique. Like the cross-correlation technique, the first step of identification is the injection of a suitable test sequence. The second step is the conversion of the measured time domain data into the frequency domain. As this will be a sampled digital system, the digital Fourier transform will be used. (12)

$$x[n] = \frac{1}{N} \sum_{k=0}^{N-1} X[k] e^{j\left(\frac{2\pi}{N}\right)kn} \quad n = 0, 1, 2, \dots, N-1 \quad (12)$$

By applying the DFT to the sampled voltages and currents, the system response at distinct frequencies can be identified. Knowing the system voltages and currents over the injected frequency range means that the system impedances can easily be calculated by Ohm's law. As the values returned from the DFT are complex in nature, it is necessary to

do a final conversion to find the magnitude (13)

$$Magnitude = \sqrt{(\text{RealPart})^2 - (\text{ImaginaryPart})^2} \quad (13)$$

With these values, a classical Bode plot can be formed by plotting the magnitude versus frequency on a semilog axis. From here, the desired impedance, such as inductance, can be calculated through means that will be discussed in Chapter 4. Of particular importance are filtering and averaging techniques required to get reliable values from measured data.

CHAPTER 4

IMPLEMENTATION

This chapter focuses on the implementation of the previously discussed techniques of identification. First, a generalized identification routine is developed. This routine is meant to serve as a template for identification of any type of system impedance. Next, data fitting algorithms are discussed in detail. Finally these routines are simulated for two separate converter topologies using MATLAB and Simulink. A level-two MATLAB s-function has been created to achieve the RPWMII algorithm and can be found in Appendix A. This s-function allows for variations in the switching frequency and the random frequency range to be tested. All simulations are carried out in the fixed time step mode to provide evenly spaced sampled data. Simulation times are set to at least 50 times faster than the desired switching frequency to provide the best results. As the RPWMII s-function is counter based, these very low simulation steps provide more accurate switching at the cost of increased simulation times. The data output from the fixed step mode will be equivalently sampled at a sampling frequency equal to the inverse of the simulation time. This sampling frequency will be on the order of several megahertz, much higher than in a realistic implementation, so down sampling of the data will be done after the simulations are complete. Setting the simulation time to even multiples of the desired sampling frequency also makes the future down sampling simpler. Processing the sampled data after simulations instead of during the runs allows for faster simulations as well as the ability to test several different filtering methods and

sample times. As the simulations tend to be long, roughly 500 times slower than real-time, this method has the added benefit of gathering data once and executing the relatively fast post processing with varying parameters.

4.1 Identification Routine

Until this point, the methods of identification have been discussed in general terms without a defined identification routine. This section is meant to develop a standard procedure that can be used to identify any type of impedance in the system. The first step is to measurement the necessary voltages and currents. The selection of the sampling frequency is important as it will limit the maximum identifiable frequency to $F_{sample}/2$ by the Nyquist criterion. Care must be taken to set this sampling frequency well enough above the injection frequency range to ensure accurate impedance estimation. In the case of the following simulations, a sampling frequency slightly higher than twice the maximum injected frequency ensures the widest sampled band of data possible. Next, the FFT of the sampled voltages and currents must be taken to transform the sampled time domain data into the frequency domain. With this frequency domain data, the complex impedance can be calculated using Ohm's Law by simply taking the ratio of the FFT voltage and FFT current. Taking the magnitude of this resultant complex impedance yields the magnitude of the measured impedance. As the RPWMII injects frequencies over a known range, this is the series of frequencies over which a numeric impedance estimation will be made. At this point, there are two possible methods (discussed in detail below) for calculating a numeric value for the circuit parameter in question. Both methods rely on using the measured impedance to solve the known impedance equation of the device of interest. For example, if the impedance in question is an RC circuit with

a known resistor value, capacitance can be calculated using the measured impedance data, the frequency at that impedance value, the known resistor value, and the equation for the magnitude of the impedance. This general methodology is shown here. (Figure 4.1)

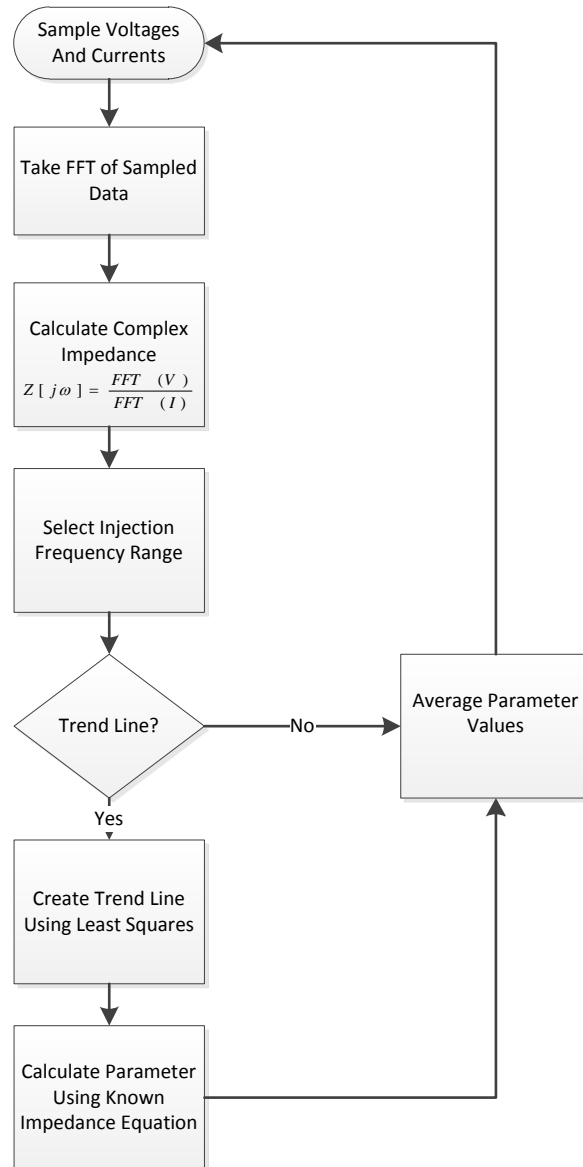


Figure 4.1 General methodology for impedance calculation

4.2 Measured Impedance Averaging

The first method of numeric impedance calculation is to average a large number of calculated values over the injected frequency spectrum. With this method, the parameter in question, for example capacitance, is calculated for each frequency within the injected range. This vector of values can then be averaged to yield an approximate value for the measured capacitance. This method relies on the RPWMII injection to provide ample data within the frequency range. The averaging routine could be optimized for a real controller by implementing concepts such as a moving average. This technique does require several calculations, defined by the number of points selected within the injected frequency range. An example of this technique can be found in Section 4.4 where the inductance value of a Buck converter is calculated.

4.3 Least Squares Fitting

While the previous method does show promise for numeric impedance approximation, the results rely on the average of a large number of values for best results. If large outliers are present in the reconstructed impedance plot, the results can be skewed, leading to a higher percentage of error. For this reason, the improved method of identification will utilize a trend line step before the parameter calculation routine. This trend line calculation will help eliminate the large outliers. One such trending algorithm is Linear Least Squares fitting. [14] The least squares method attempts to minimize error in a signal and is common for data fitting. This procedure uses the measured data over the injection range to calculate a Y-intercept, b , and a slope, m , that will form the trend line. (14,15,16)

$$b = \frac{\sum Y \sum X^2 - \sum X \sum XY}{n \sum X^2 - (\sum X)^2} \quad (14)$$

$$m = \frac{n \sum XY - \sum X \sum Y}{n \sum X^2 - (\sum X)^2} \quad (15)$$

$$y = mx + b \quad (16)$$

For the purpose of impedance reconstruction, X represents frequency while Y represents the measured magnitude. Once the impedance magnitude has been calculated, the values for the trend line are determined. The values on this trend line are then the values used to calculate the desired parameter in question. While this method is essentially adding another step to the calculation process, it has shown to improve the results and minimize the percent error. The MATLAB function used for this trending portion can be found in Appendix C.

4.4 Buck Converter

The buck converter is one of the most common types of converters used for stepping down one DC voltage to a lower DC level. [15] While there are several possibilities as far as switching elements (MOSFETs, diodes, or IGBTs) here ideal switches are shown. (Figure 4.2)

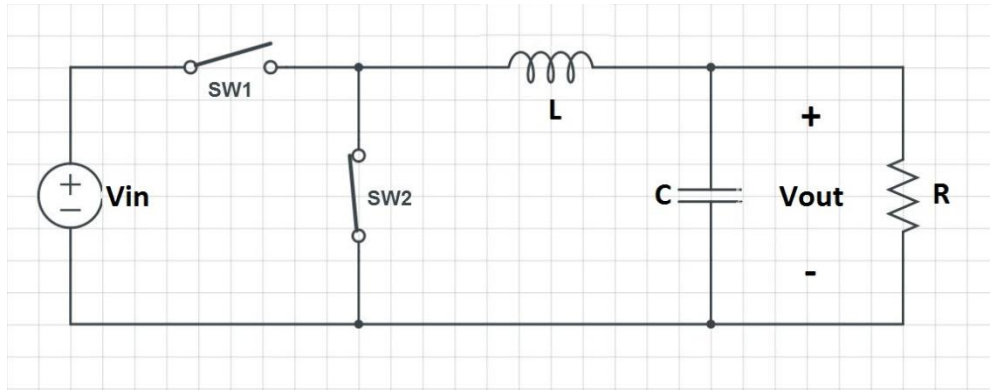


Figure 4.2 Buck converter with ideal switches

Buck converters accomplish their voltage regulation through control of the switched current seen by the inductor. By varying the amount of time the upper switch is on in relation to the lower switch, the output voltage level can be controlled. At the switching node, the voltage produced is a square wave with a frequency equal to the switching frequency. When viewed as a sum of sinusoids, it is clear to see that this square wave will inject noise at the fundamental switching frequency as well as its numeric harmonics. Here, an arbitrary square wave is shown along with its first three sinusoidal components. (Figure 4.3)

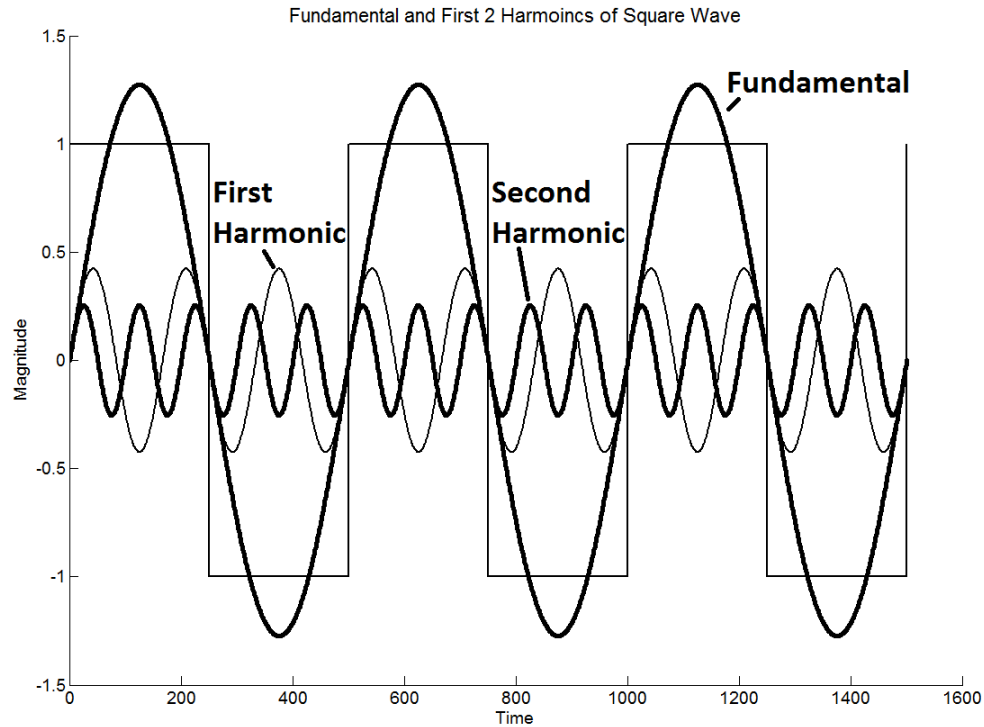


Figure 4.3 Square wave with harmonics

To achieve the desired DC output voltage, a low pass filter is formed by the inductor and capacitor. Careful selection of these filter elements can reduce the hard switching square wave to a DC value with minimal voltage ripple. This type of converter often senses the switched current as well as the output voltage making it possible, through the aforementioned methods, to identify the inductor's value.

The buck converter simulation is carried out using MATLAB and Simulink. As can be seen, the high side switch is realized through an ideal switch while the low side consists of a diode. (Figure 4.4) Common component parasitics such inductor and capacitor series resistances have been included to more closely match a realistic converter.

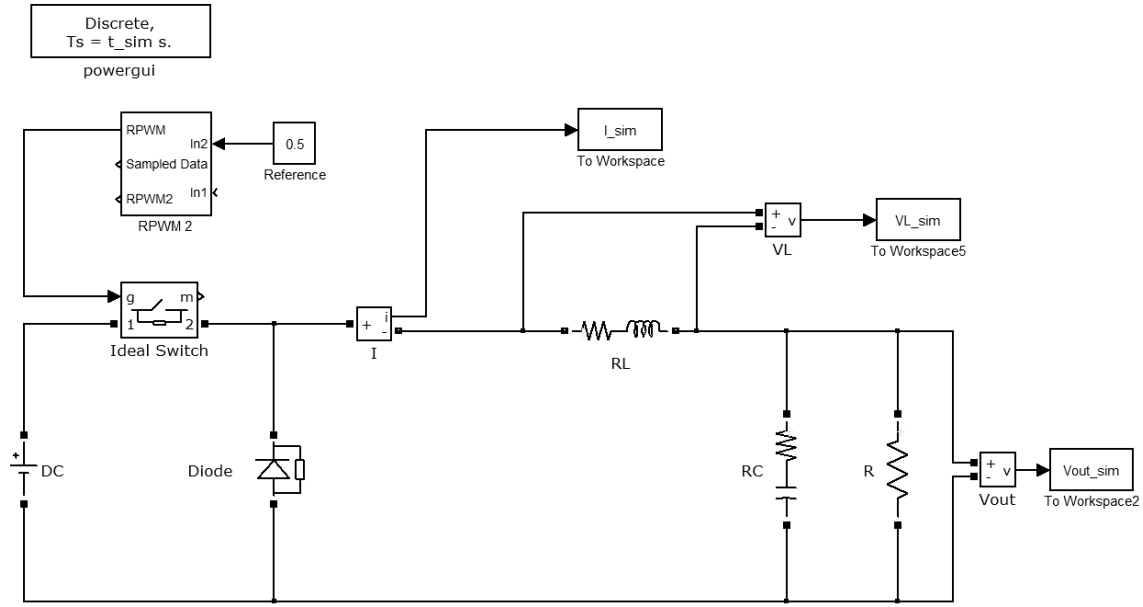


Figure 4.4 Buck converter used for simulation

As can be seen in the schematic, measurements are made and saved to the MATLAB workspace for inductor current, inductor voltage, and output voltage. It should be noted that in a physical implementation, the differential inductor voltage is not measured directly, but could be reconstructed by taking the difference of the output voltage and the known switching state. This allows for the possibility of measuring several different system impedances as validation of the concepts of impedance identification. Before implementing RPWMII, a control simulation is run using standard DPWM. All important simulation values can be found in Table 4.1. Outputs are down sampled to a 24 kHz sampling rate to reflect a more realistic sampling frequency. For this reason, the maximum identification frequency is $F_{sample}/2$ or 12 kHz.

Table 4.1 Simulation Values for DPWM Buck Converter

Variable	Value
Simulation time	8.3333e-007 seconds
Switching Frequency	8kHz
Input Voltage	15V
Duty Cycle	50%
Inductance	330 μ H
Inductor ESR	0.1 Ω
Capacitance	400 μ F
Capacitor ESR	0.1 Ω
Load Resistance	8.6 Ω

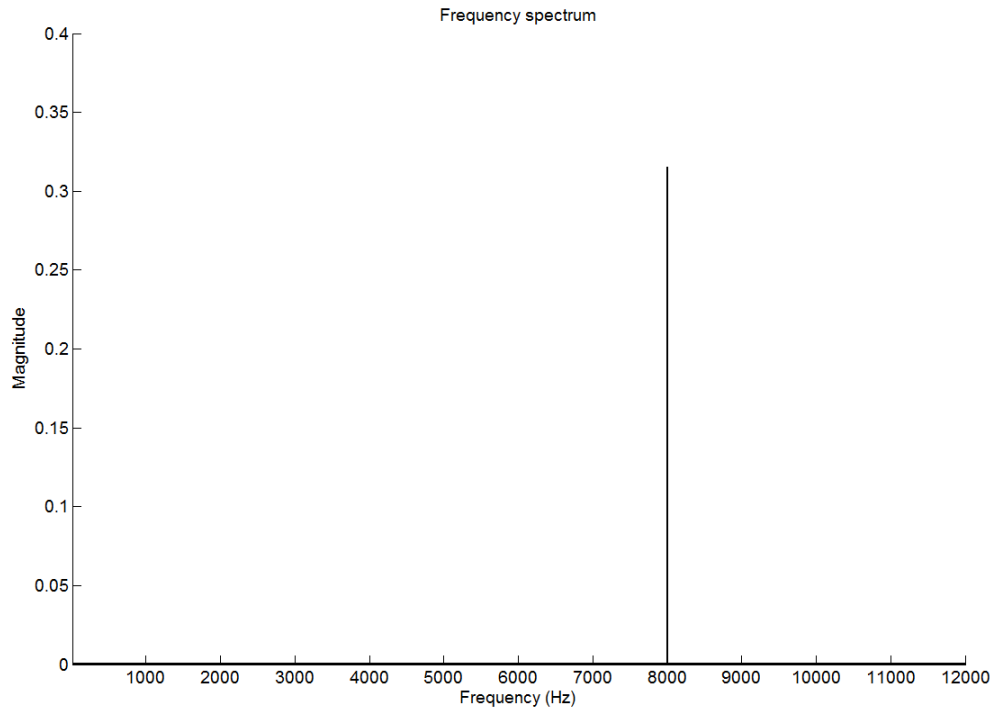


Figure 4.5 Current frequency spectrum of DPRM buck converter simulation

Due to the set switching frequency, the measured current spectrum has a characteristic spike at 8 kHz. (Figure 4.5) Next, a simulation is run using the custom RPWMII s-function block. Here, all component values have been kept the same, the only difference is the switching frequency will not vary over the range of 4000 to 9000 Hz. The current frequency spectrum shows the dramatic reduction in large harmonic spikes. (Figure 4.6) Note that when comparing Figure 4.5 and 4.6, different scales are used for the Y-axis. This was done to help show the general shape of the injected frequency spectrum for the RPWMII simulation.

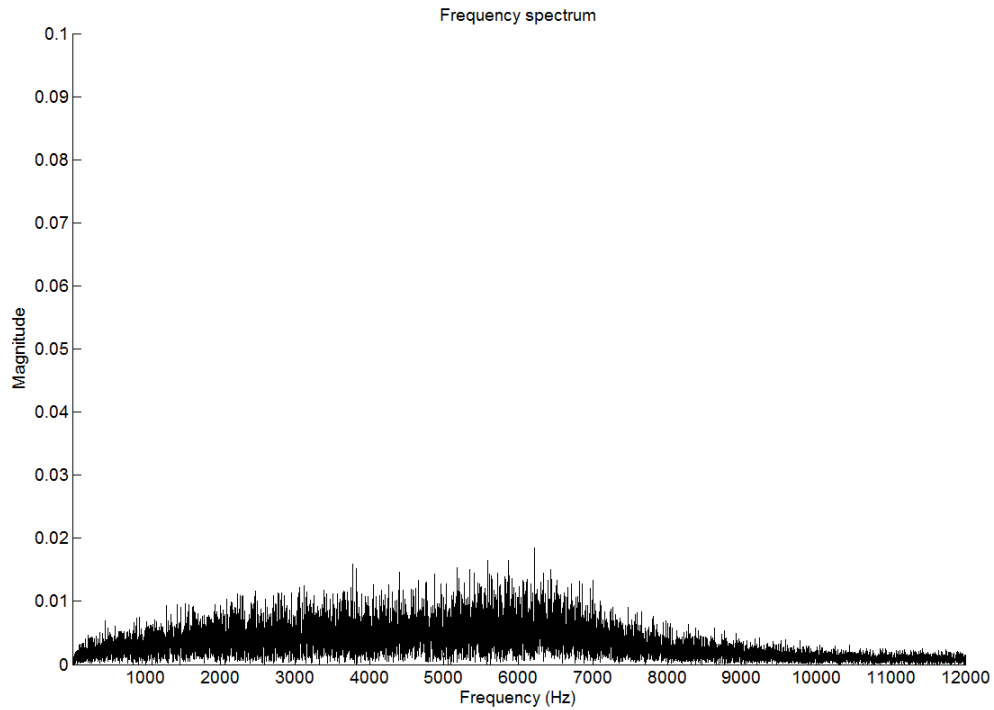


Figure 4.6 RPWMII current frequency spectrum

If we try to construct an impedance plot using the output voltage and measured current we would expect to see the parallel combination of the filter capacitor and it's ESR with the output resistance. In terms of $j\omega$ this impedance would be

$$Z(j\omega) = \frac{j\omega C R R_{ESR} + R}{1 + j\omega C R_{ESR} + j\omega C R}$$

The Bode plot of this function shows the characteristic downward slope attributed to the capacitor that eventually begins to flatten due to the ESR. (Figure 4.7)

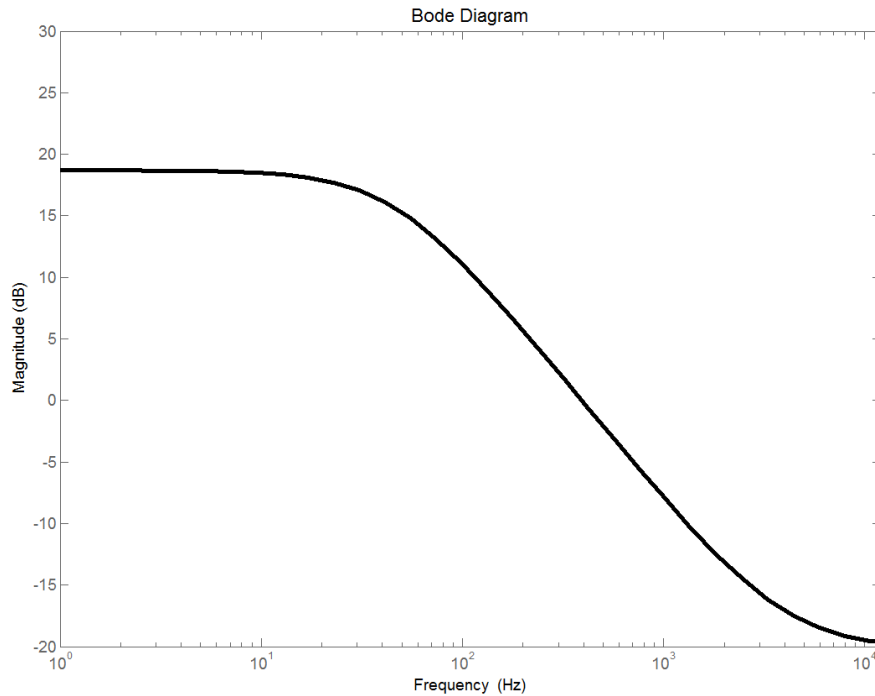


Figure 4.7 Expected Bode plot for $Z(j\omega)$

Using the measured output voltage and inductor current from the RPWMII simulation, a fairly accurate impedance reconstruction can be made. (Figure 4.8) As can be seen in the plots, most of the salient features of the transfer function can be observed including the load resistance, ESR, and the capacitor induced slope. It is important to note that the tightest reconstruction occurs around the injection frequency range and tends away as the frequency approaches zero. It can also be seen that there is a fair amount of noise present in the form of substantial outliers.

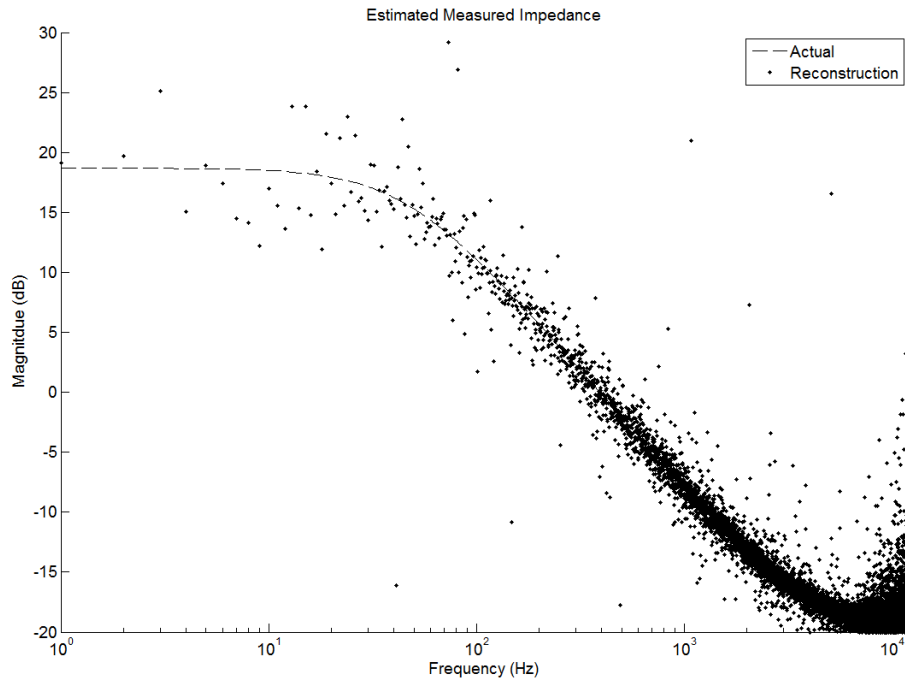


Figure 4.8 Constructed impedance using RPWMII

To minimize these erroneous data points and provide a tighter reconstruction, the averaging step is used. The averaging routine improves with the number of sampling periods used at the cost of increased calculation time. The results of the averaging function, found in Appendix B, show a much tighter reconstruction about the actual impedance. Here, the same impedance is recreated while sampling the FFT over two sample lengths. (Figure 4.9) As can be seen, most of the outliers have been eliminated, and the impedance plot looks much closer to the actual expected value.

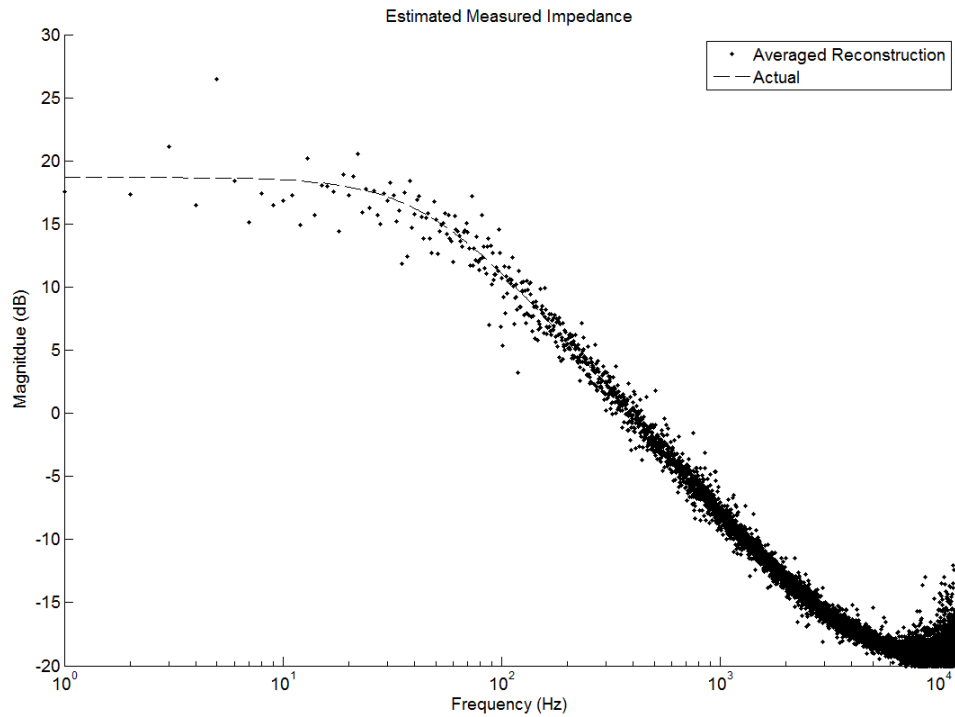


Figure 4.9 Constructed impedance using RPWMII and averaging

While this impedance reconstruction is interesting, for the sake of controls we would prefer to identify the inductor element. The same simulation data is used, but this time we will take the FFT of the inductor voltage. When the same process of averaging is used the following Bode plot is generated, showing the measured and actual value for an RL circuit given the same component values as the simulation. (Figure 4.10)

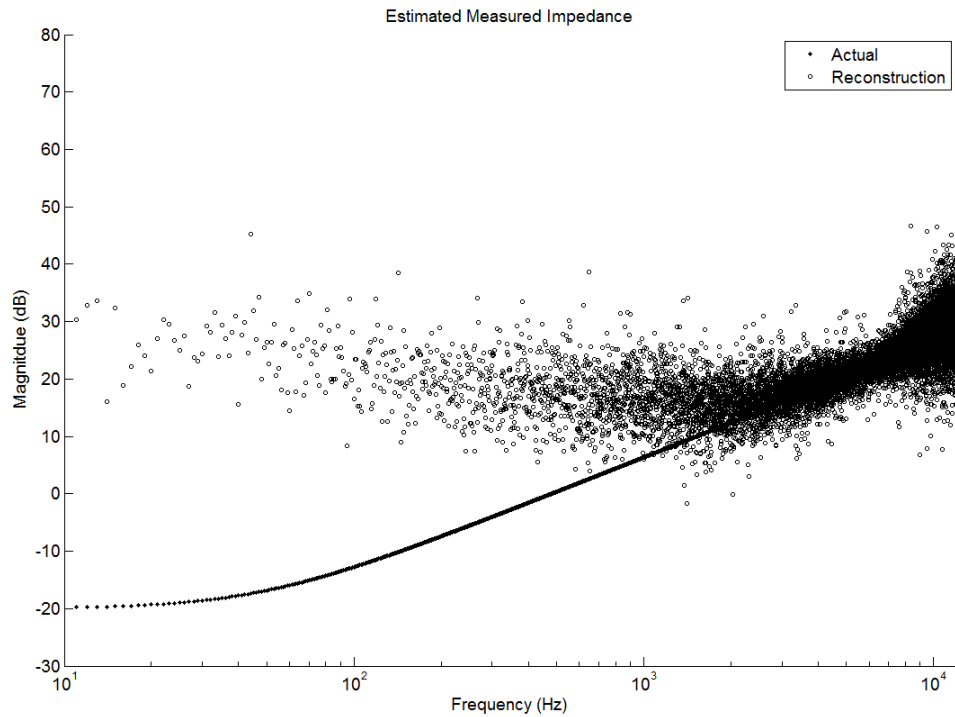


Figure 4.10 Constructed RL impedance using RPWMII and averaging

As can be seen, outside of the range of frequencies injected by the RPWMII signal, the measured impedance quickly trends away from the actual value. If we look at just the range of injected frequencies, here 4 kHz to 9 kHz, the matching is much clearer. (Figure 4.11)

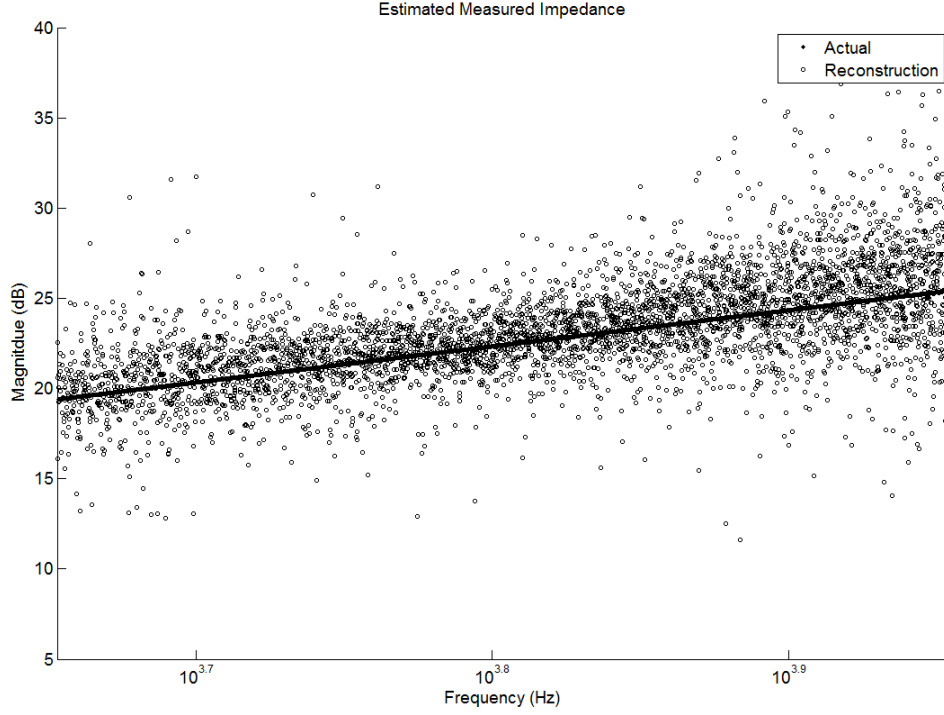


Figure 4.11 Constructed RL impedance using RPWMII and averaging ZOOM

Since it is desired to have a numeric value for the measured inductance, it is necessary to perform a fitting algorithm to the measured impedance plot. For this parametric fitting there are essentially two variables, the inductance and the built in resistance of the inductor. If the rated inductor resistance is considered a constant, a fairly accurate approximation of the inductance can be made by using the equation for the magnitude of the RL impedance. (17)

$$|Z(j * 2\pi * f)| = \sqrt{R_L^2 + (j * 2\pi * f * L)^2} \quad (17)$$

Solving (17) for L leads to the following equation (18) which contains one unknown (L), two known values (R_L and f), and one measured value ($|Z(j * 2\pi * f)|$).

$$L = \sqrt{\frac{(|Z(j*2\pi*f)|)^2 - R_L^2}{4*\pi^2*f^2}} \quad (18)$$

With (18) it is possible to calculate the unknown inductance by using the impedance magnitude from the reconstruction step and the known inductor resistance. The inductance calculation begins by slicing just the frequencies of interest. This is a simple step as the results of the FFT are stored as an array of magnitudes versus frequency, and the injected frequency range is selected during the design phase of the controller. Next, the inductance is calculated at each frequency within the range. It should be noted that it is not necessary to iterate through each frequency over the range, but a higher number of points used will result in a better average. Careful design of the final code would also allow for a somewhat parallel solving structure where the inductance value is being calculated while the next set of voltages and currents are being sampled.

Multiple simulations confirm the viability of this averaging technique for identifying the system inductance assuming a constant inductor resistance value. Three separate simulations show that the inductance value can be found with less than 10% error. (Table 4.2) For each simulation the frequency range for inductor averaging has been selected to be 5 kHz to 6 kHz as it falls within the heart of the injected frequencies.

Table 4.2 Simulation Results for Inductance Calculation

Actual Value	Calculated Value	Percent Error
165μH	176μH	7.1%
330μH	345μH	4.5%
660μH	695μH	5.3%

Though it is outside the scope of this research, these calculated inductance values could then be used to update the inductance value used within the closed loop controller. The literature has shown the improvements possible when the inductance can be updated in real time. [16]

4.5 Single Phase Grid-Tied Converter

The next converter of interest is the single phase grid-tied converter. The grid-tied converter can easily be implemented as an active rectifier, an inverter, or for use with energy flow management. The single phase case is used as it reduces the number of measurements necessary and serves as a good approximation for the balanced three phase converter. (Figure 4.12) For an actual implementation, special care will be needed to ensure the proper voltages are measured. [17]

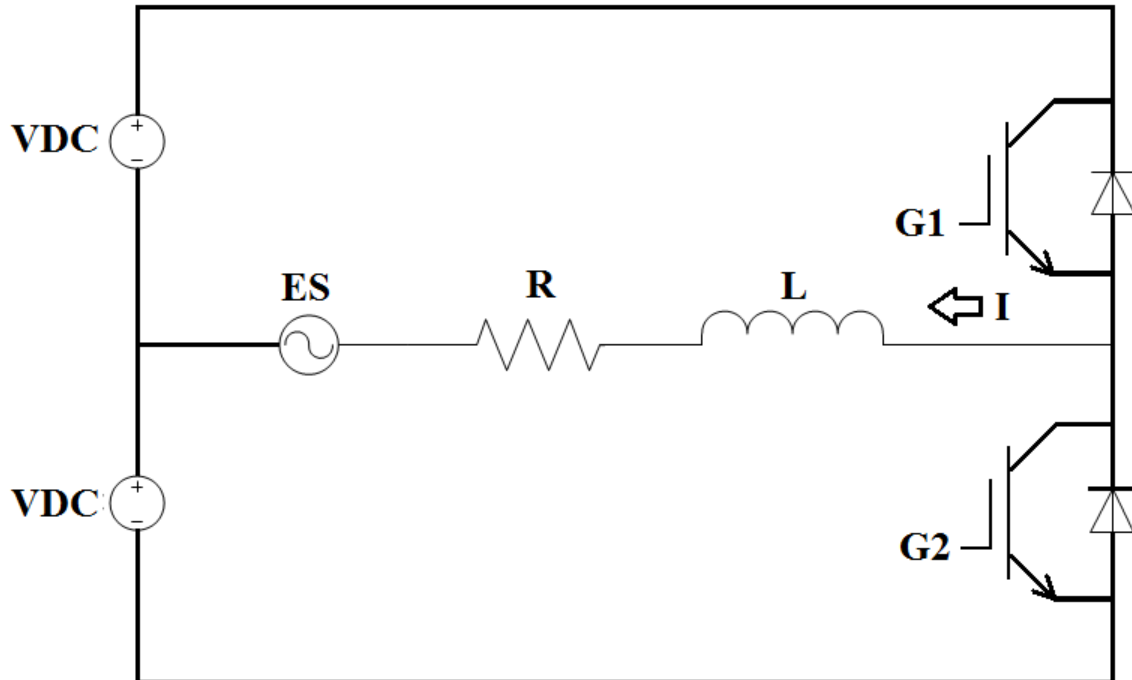


Figure 4.12 Single phase, grid-tied converter

The process of identification is similar to that used for the DC-DC buck converter, the difference being there will now be additional low frequency harmonics present in the system. These harmonics arise due to the fact that there is now a sinusoidal voltage and current being produced. This fundamental frequency is often much lower than the switching frequency, and in this simulation it will be set at 60Hz to match the US power grid. (Figure 4.13)

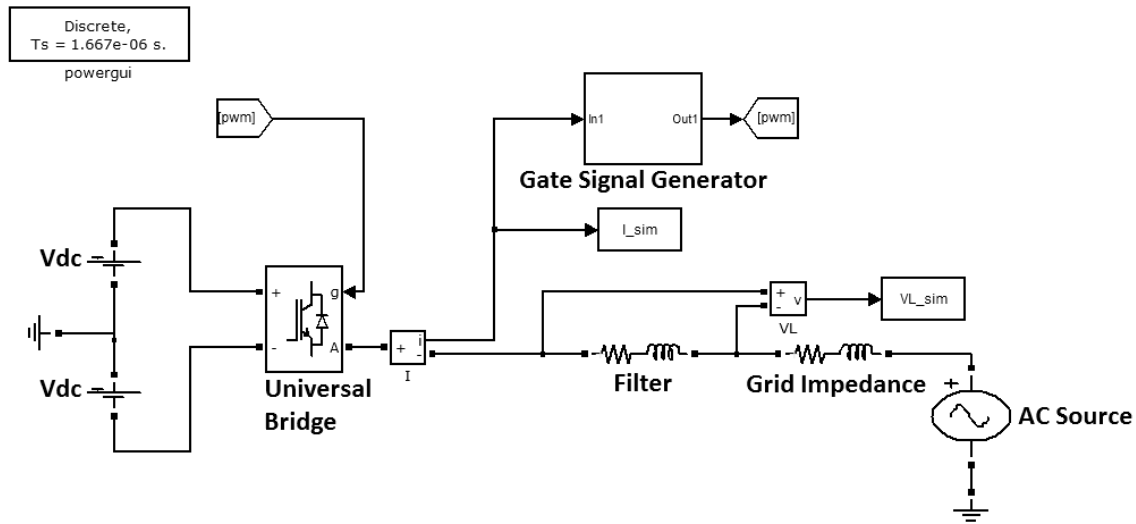


Figure 4.13 Grid-tied converter simulation

As with the Buck converter, the first simulation uses a standard DPWM to serve as a baseline. A one-arm universal bridge is used with the gate signals generated by a CBPWM. The grid is simulated by an AC voltage source with a resistive-inductive grid impedance. All relevant simulation values are listed in Table 4.3. The current spectrum contains the typical spike at the switching frequency, but now there are also frequency contributions from the fundamental of the grid frequency. (Figure 4.14)

Table 4.3 Simulation Values for DPWM Grid-Tied Inverter

Variable	Value
AC source maximum amplitude	300 V
AC source frequency	60 Hz
Grid Inductance	1 mH
Grid Resistance	10 m Ω
Filter Inductance	10 mH
Filter Resistance	28 m Ω
Switching Frequency	8 kHz

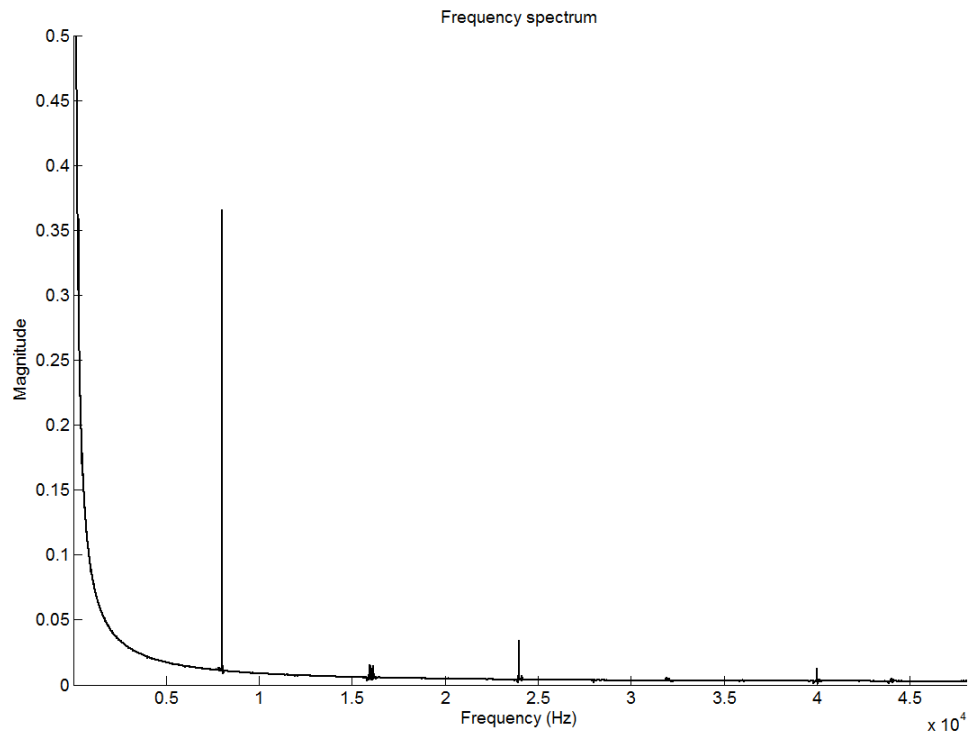


Figure 4.14 DPWM inverter simulated current frequency spectrum

The DPWM is then replaced with the custom RPWMII block with an injection range of 5 kHz to 9 kHz. As expected, the large spike at the switching frequency has been replaced by a wide spectrum frequency injection. (Figure 4.15) The frequency reconstruction also shows a much closer fitting to the actual impedance value within the injected frequency range. (Figure 4.16) Using the same method as that used for the buck converter, a numeric value is found for the filter inductance.

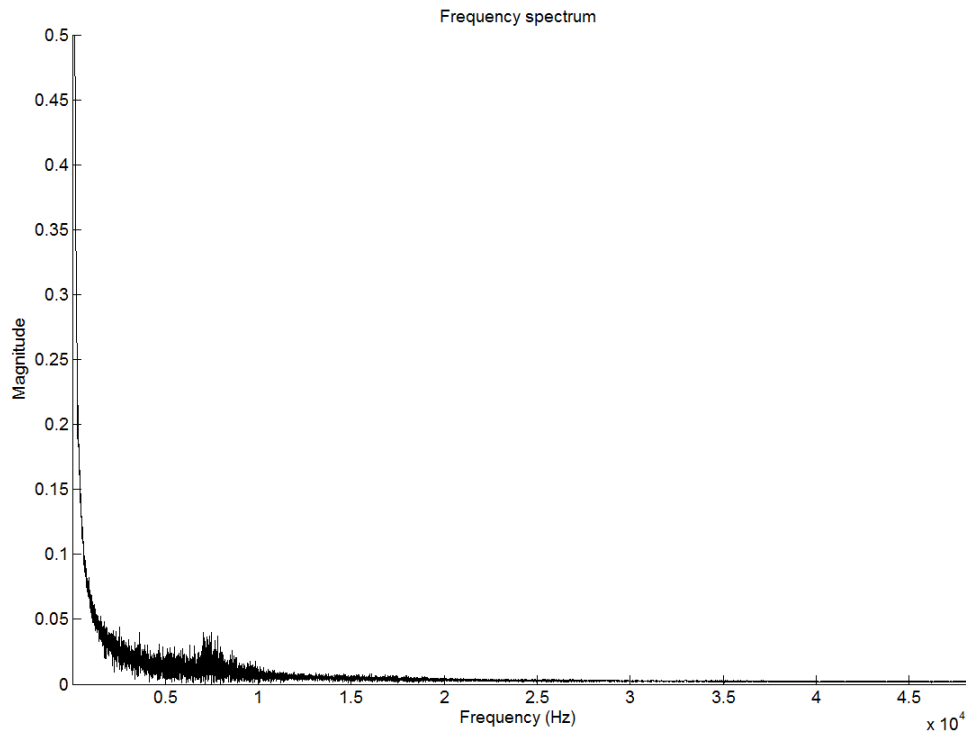


Figure 4.15 RPRMII inverter simulated current frequency spectrum

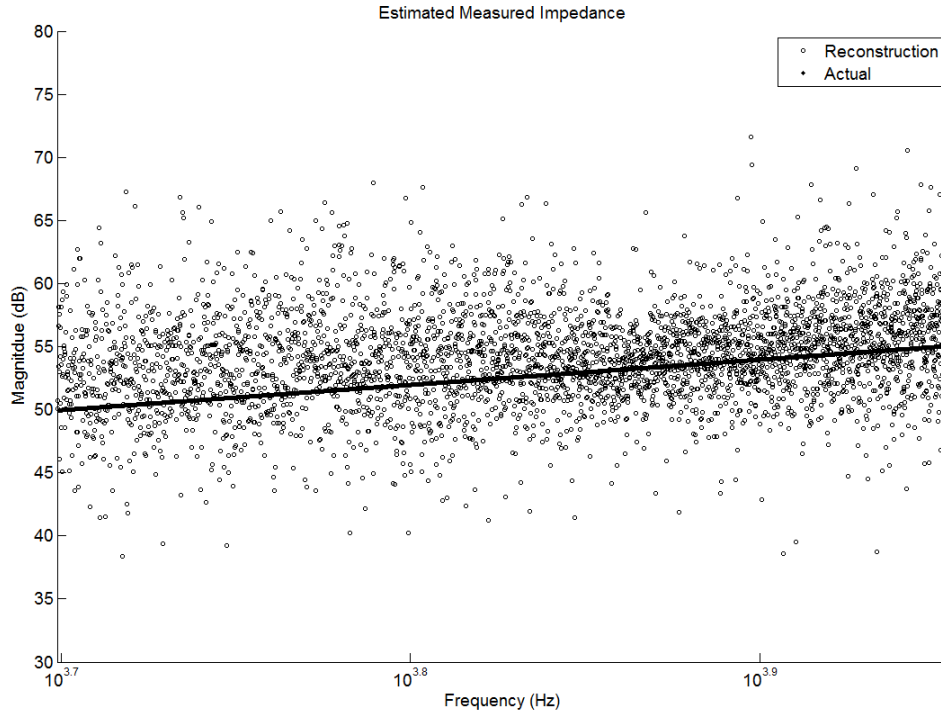


Figure 4.16 RPWMII Inverter impedance reconstruction ZOOM

Several simulations confirm the viability of these methods for inductance estimation using RPWMII. Table 4.4 shows the calculated versus real values and compares the averaging method with the least squares fitting method.

Table 4.4 Improvements Using Least Squares Fitting

Simulation	Calculated Without Fitting (percent error)	Calculated With Fitting (percent error)
R=28m Ω L=10mH	10.7 mH (6.9)	10.4 mH (4.8)
R=28m Ω L=5mH	6.0 mH (21.2)	5.6 mH (11.4)
R=28m Ω L=2mH	2.5 mH (23.0)	2.3 mH (12.8)
R=1 Ω L=10mH	10.9 mH (9.6)	10.4 mH (4.8)

As can be seen, the methods developed for the Buck converter also work very well for the grid-tied converter. The frequency components created by the grid fundamental do little to corrupt the estimated impedance value as they exist much lower than the range of identification frequencies.

CHAPTER 5

HARDWARE VALIDATION

To confirm the findings of the simulation, a low power Buck converter has been built to closely match the one in simulation. Special consideration has been made when selecting components to account for parasitics. Each passive component is measured with an Agilent U1733C LCR meter over a range of frequencies with the average results found in Table 5.1.

Table 5.1 Actual Component Values for Buck Converter

Component	Rated Value	Measured Value
Inductor	330 μ H	333 μ H
Inductor DC Resistance	N/A	0.54 Ω
Capacitor	470 μ F	420 μ F
Capacitor ESR	N/A	0.23 Ω
Load Resistor	10 Ω	10.1 Ω

The controller used is the PIC32MX460F512L-80I/PT from Microchip built on a custom carrier board. This particular controller can operate up to 80 MHz which will allow for finer resolution of the generated RPWM. The onboard ADCs will not be used as the excess overhead necessary would quickly outpace the abilities of the controller. Instead, the necessary measurements are made using a Labview NI-USB-6009 14-bit data acquisition unit. This particular model is capable of sampling two channels at a maximum

rate of 24 kHz which is in line with the simulations. The use of the data acquisition unit has the added benefit of being able to easily export the measured data in a format that can be read by MATLAB. This means that the same fitting code used for the simulations can be used on the measured data. Voltage is measured directly while the current is measured using the ACS712ELCTR-30A current sensor on a custom made sensor board. (Figure 5.1)

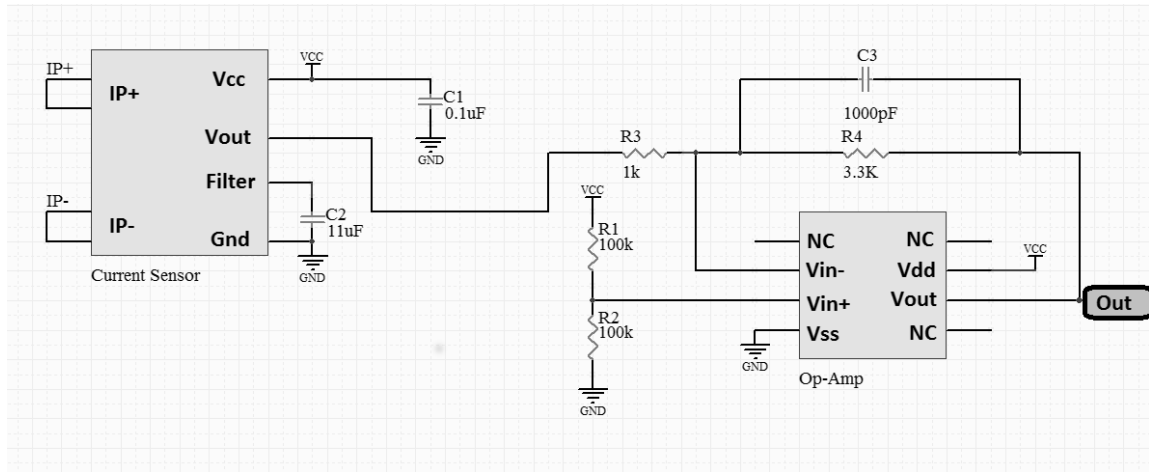


Figure 5.1 Current sensor schematic

To match the simulations, the first impedance measured is the parallel combination of the output capacitor and load resistor. The following plots show the measured reconstruction of the selected impedance versus the actual impedance for two different capacitor values. (Figure 5.2 and Figure 5.3)

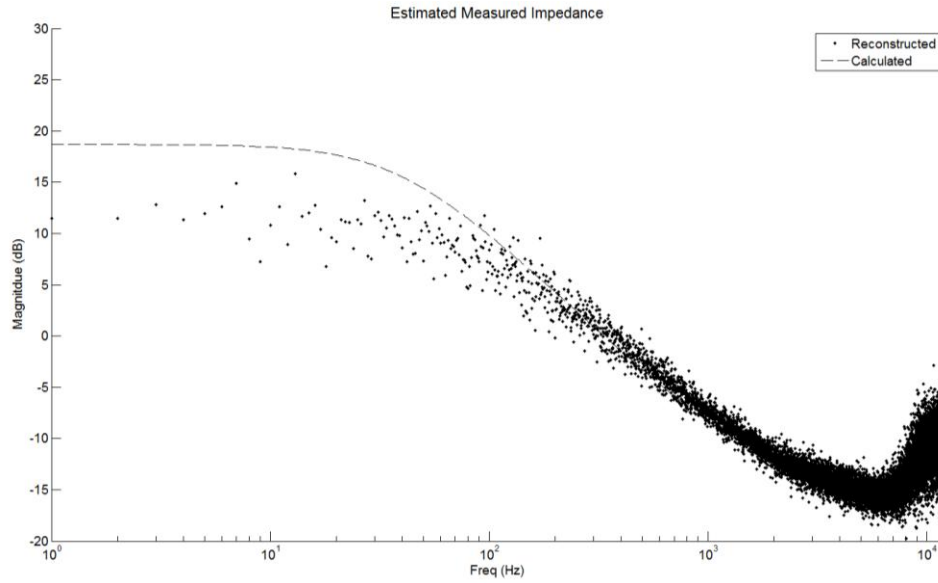


Figure 5.2 Hardware validation $C = 470\mu\text{F}$

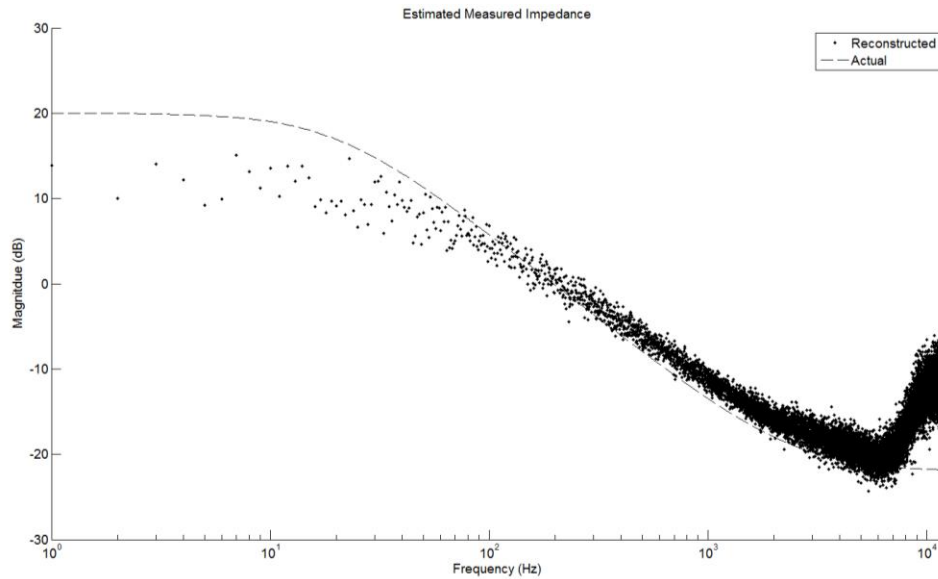


Figure 5.3 Hardware Validation $C = 800\mu\text{F}$

Much like the simulations, both reconstructions follow the actual impedance very closely. The change in corner frequency as well as the difference in ESR is clearly visible. The frequency spectrum of the measured current shows the characteristic signs of the spread spectrum noise expected from the RPWMII simulations. (Figure 5.4) It should

be noted that while there is a spike on the frequency spectrum, its magnitude is relatively small and is most likely caused by the limited resolution of the controller's RPWM sequence. In terms of impedance measurement, its presence goes unnoticed.

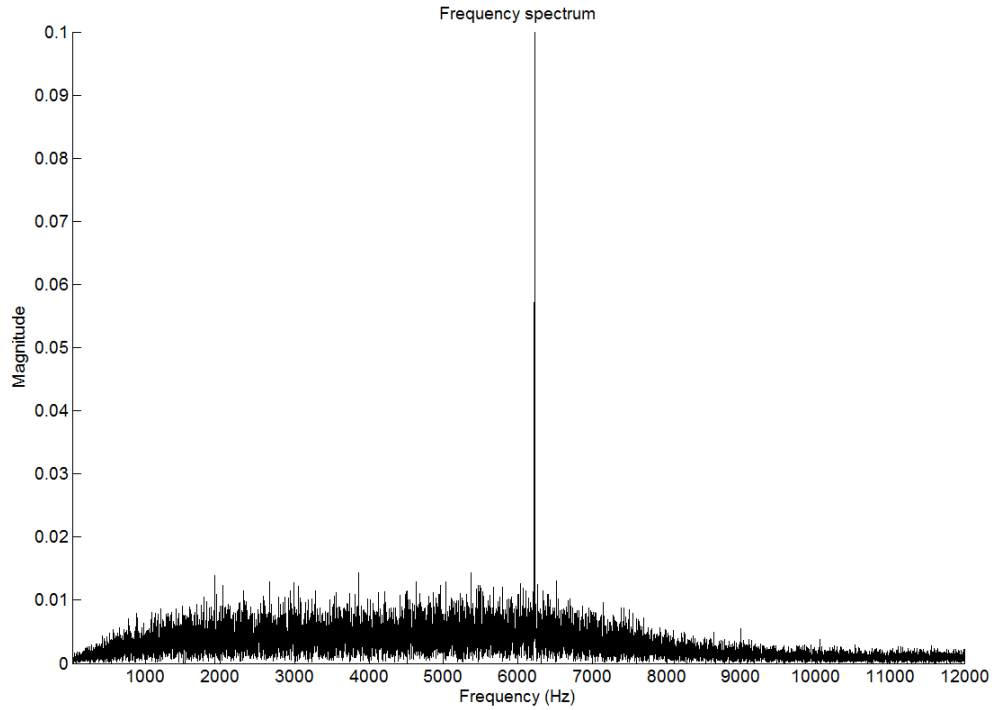


Figure 5.4 Measured current frequency spectrum

Next, the previous methods for inductor estimation are used to calculate the value of the real components. It is important to note that while the inductor voltage could be determined by the known converter switch states and output voltage, here a differential voltage measurement is made across the inductor. For the particular data acquisition unit used, the sampling frequency for three channels (current, output voltage, and switched voltage) reduces the maximum sampling frequency to 16kHz. This in turn limits the maximum identifiable frequency to 8kHz. Below are the impedance reconstructions using two separate inductor values, showing just the range of injected frequencies. (Figure 5.5 and Figure 5.6)

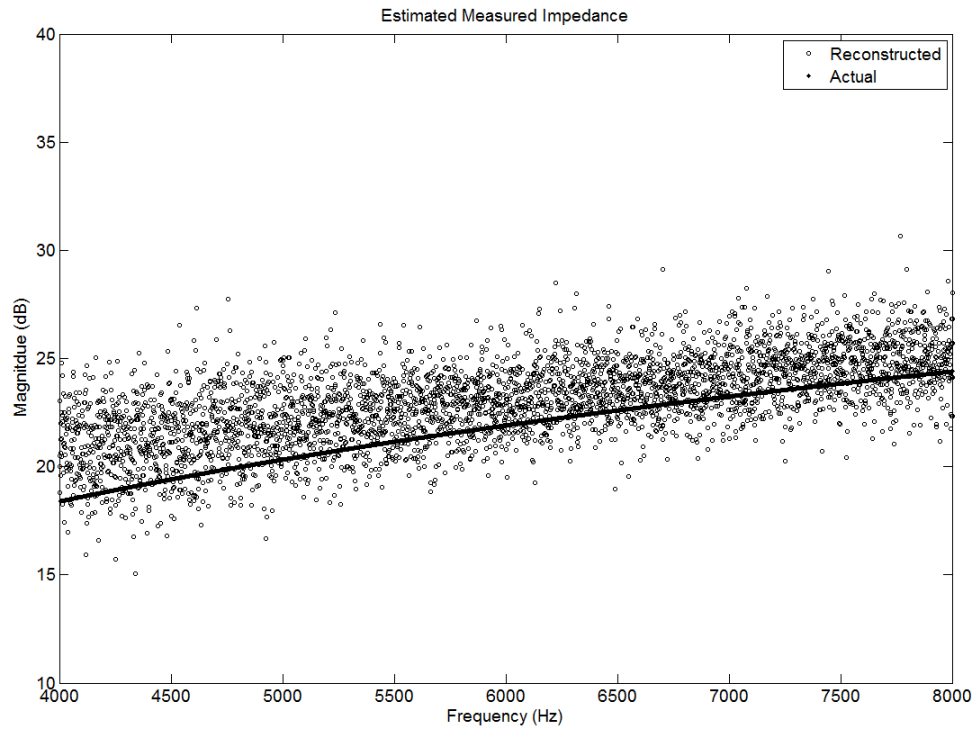


Figure 5.5 Impedance reconstruction with $L=330\mu\text{H}$

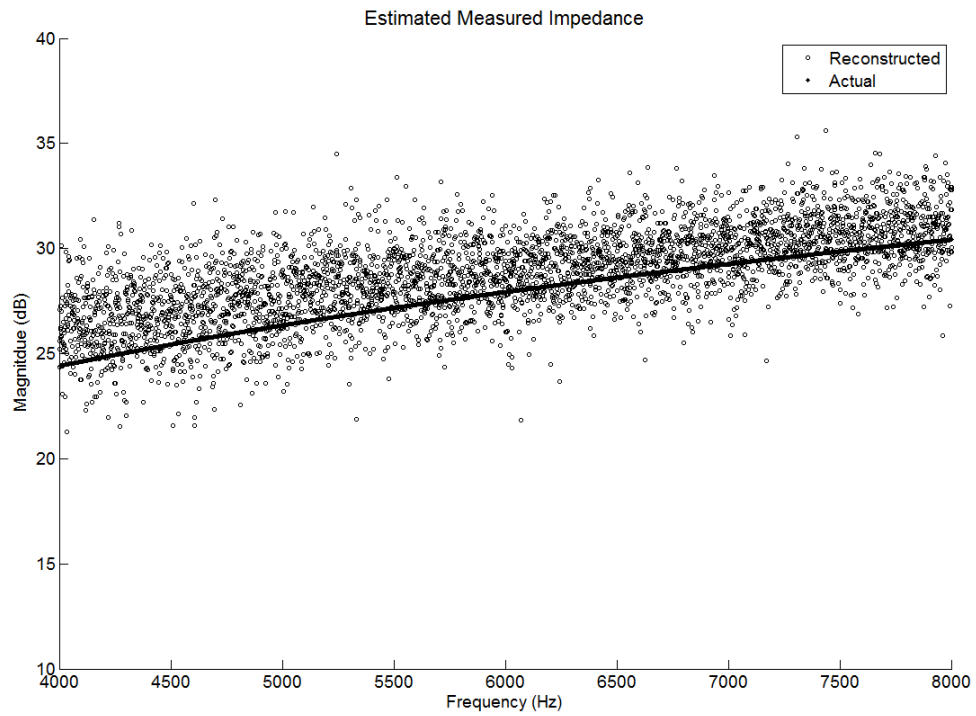


Figure 5.6 Impedance reconstruction with $L=660\mu\text{H}$

These impedance reconstructions show a close matching to the expected actual values. When numeric values for inductance are calculated, the results are very promising. (Table 5.2) Factors such as measurement error have been eliminated as much as possible by calibrating the sensors against known voltage and current sources.

Table 5.2 Calculated Inductance Values

Rated Inductance	Calculated Without Fitting (percent error)	Calculated With Fitting (percent error)
330 μ H	372 μ H (12.6)	367 μ H (11.3)
660 μ H	728 μ H (10.4)	719 μ H (9)

CHAPTER 6

PRACTICAL CONSIDERATIONS FOR IDENTIFICATION

The goal of this thesis is to develop a method for impedance identification for real systems. That makes it necessary to consider practical limitations of the system when developing these procedures.

6.1 Sampling Time and Frequency

As the DFT is a summation of multiplications, it can quickly become computationally taxing. For this reason, fast Fourier transforms will be used. The FFT is able to reduce the number of operations to $(N)\log_2 N$ as opposed to N^2 for the more general Fourier transform. [18] Most modern digital signal processors contain highly efficient FFT functions that simplify the implementation of these techniques. The total execution time of the FFT algorithm is determined by the processor execution time, and the length of the sampled data. Table 6.1 demonstrates the time savings possible by using the FFT over the standard Fourier transform.

Table 6.1 Execution Comparison Between Fourier Transform and FFT

Number of Samples	Fourier Transform Number of cycles	FFT Number of cycles
128	16384	621
256	65536	1420
512	262144	3194
1024	1048576	7098

The FFT length is determined by both the system sampling frequency, and the length of the sampling period. The sampling frequency and the sampling period both play a role in the final resolution in the frequency domain. This resolution is the maximum number of Hz between any two given samples after performing the FFT and is calculated by (19)

$$\text{frequency resolution} = \frac{\text{number of samples}}{\text{sample frequency}} \quad (19)$$

This frequency resolution is important as it is one of the determining factors in the final quality of the system identification. If we consider a simple RL circuit, the frequency resolution determines the change in inductor value it would be possible to identify under ideal conditions. (Figure 6.1) In this example, a fixed resistance of 10Ω is used while the inductor value is changed from 1mH to 1.5mH. At the 3dB point of each graph, there is a difference of approximately 50Hz between the two plots. Therefore, if the goal was to distinguish between inductances of 1mH and 1.5mH at their corresponding corner frequencies, the frequency resolution would need to be at least 50Hz.

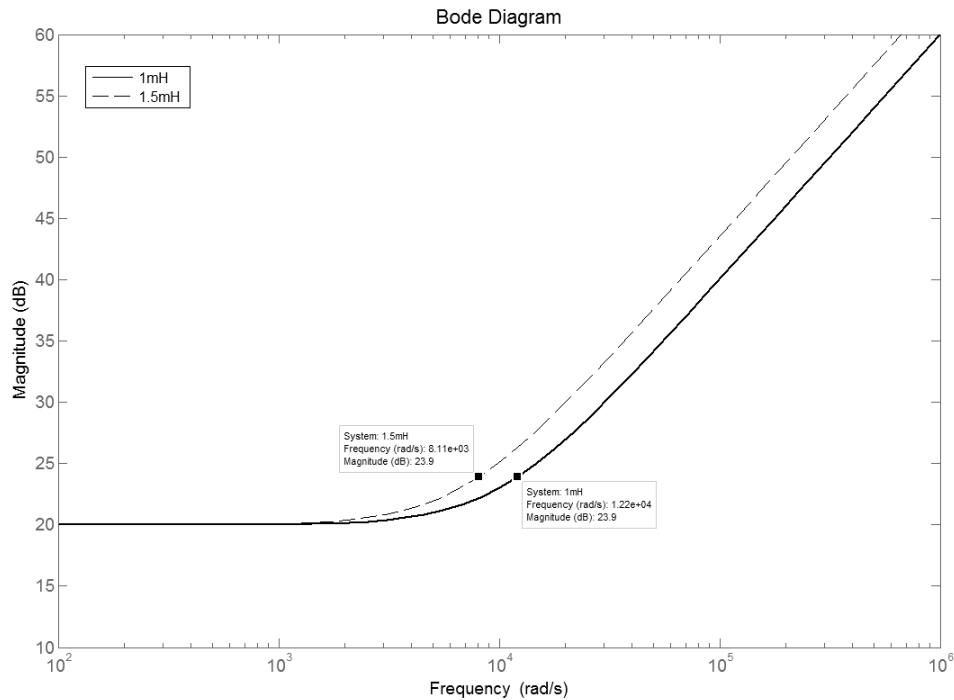


Figure 6.1 Importance of frequency resolution

Ideally, one would use the longest sample period possible to provide for the highest possible frequency resolution. Practically speaking, this sampling period is limited by two factors; how frequently identification is needed, and memory restrictions of the controller. Consequently, physical parameters of the controller as well as desired identification resolution determine the sample period length and in turn, the maximum frequency resolution.

6.2 Sampling Resolution

Another factor in determining the accuracy of identification is the precision of the measuring devices. Possible measurement error falls under two main categories: magnitude error and time or frequency error. Magnitude error encompasses factors from quantization errors within the analog to digital converter and non-linearity of the sensors

or ADC. Much like the aforementioned frequency resolution, the ability to discern between two possible impedance values is limited by the measurement resolution. The Bode plot of two simple RL circuits is shown below. (Figure 6.2) For both plots, the inductance is held constant at 1mH while the resistance is changed from 5Ω to 7Ω . It is clear to see that for frequencies in the region of 250Hz, the two magnitudes differ by only 3dB. This requires that the ADC be able to discern at least this 3dB difference to be able to identify a change in resistance of 2Ω .

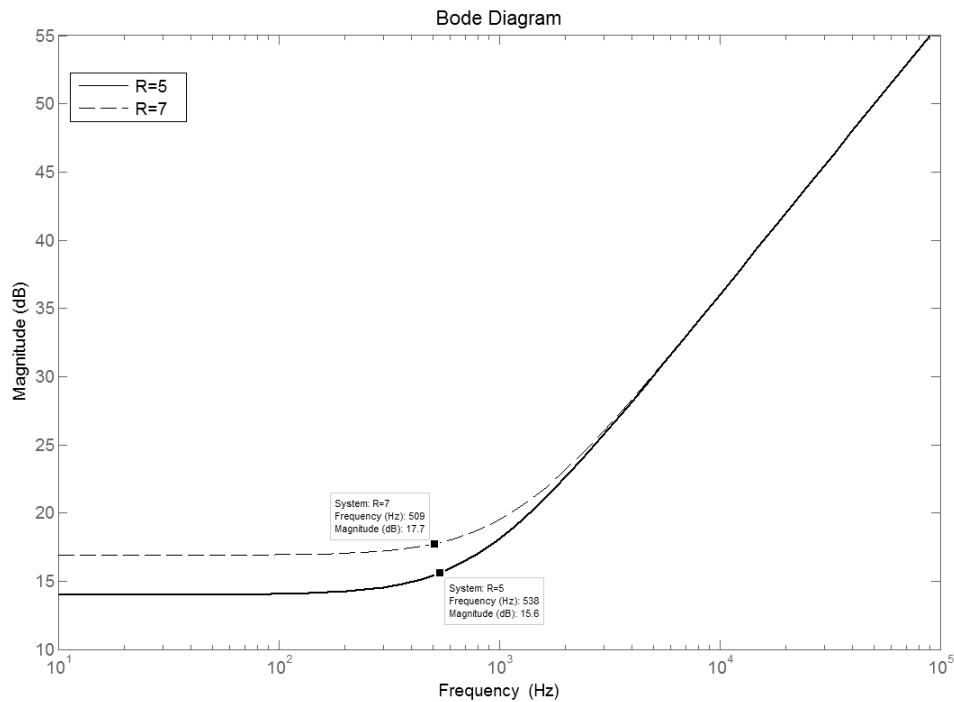


Figure 6.2 Importance of ADC resolution to identification

Not only is the relative accuracy of the measurement important, but so too is the linearity of the sensor and ADC. For simple control systems, it is often assumed that the feedback system is purely a frequency independent gain block. In reality, feedback networks contain several frequency dependent components including the sensor,

amplifiers, filters, and any system parasitics. Because the final goal of identification is to gather frequency dependent information, it is crucial that any frequency distortion introduced by the feedback network be well above the range of frequencies of interest. If the feedback loop attenuates frequencies within the identification band, the values may become too small to discern from the existing noise. For example, the ADS7863 from Texas Instruments is a dual, 12-bit ADC capable of sampling rates up to 2MSPS. From the datasheet it can be seen that with an increase in frequency there is also a decrease in the signal to noise ratio and an increase in total harmonic distortion. (Figure 6.3)

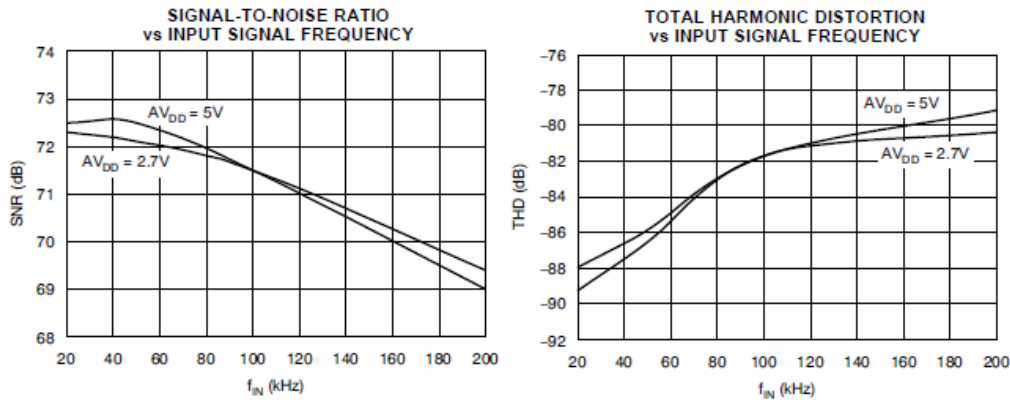


Figure 6.3 Typical ADC frequency characteristics (TI ADS7863)

When selecting components for such systems, it is important to ensure that nothing in the sensing loop will add unknown frequency distortion. As the region of interest is below the switching frequency, the feedback loop should already meet these requirements, but it is still good practice to ensure there will not be any unnecessary error introduced by the sensing loop.

CHAPTER 7

CONCLUSION AND FUTURE WORK

The objective of this work is to show the viability of using Randomized Pulse Width Modulation as a means of impedance identification in switching power converters while also minimizing the amount of harmonic noise. By monitoring the impedance of elements within the control loop, digital controllers can adapt and perform a better job of regulating the outputs. This in turn can lead to more efficient controllers, as well as the use of cheaper components that have a higher variation from their normal value as well as a greater degree of non-linearity.

The use of RPWMII as a source of accurate impedance estimation while also reducing injected harmonics has been demonstrated. Using the power converter's existing voltage and current sensors, the necessary values are sampled at a fixed frequency. Fast Fourier transforms are then used to convert this time domain data into the frequency domain. A complex impedance value can then be calculated using these voltage and currents and Ohm's law. Next, a trend line is created using the least squares fitting algorithm to help eliminate any spurious noise present in the measurements. The parameter value in question can then be solved for using the known impedance equation and the measured complex impedance over the range of injected frequencies. These methods have proven to be accurate in the estimation of impedances with DC as well as AC systems. Simulations have shown a percent error of less than 10 percent when estimating the inductance within a Buck converter and a grid tied inverter. These

simulation findings have also been validated through hardware testing on a low powered Buck converter. The concept of harmonic reduction through the use of RPWMII has also been confirmed. By spreading injected noise over a wider frequency spectrum, the large spikes common with standard switching techniques can be greatly reduced. This achieves the desired goal of converter element impedance estimation while simultaneously reducing harmful harmonic injections.

Future Work

As the main focus of this research is on the development of the use of RPWMII for impedance estimation, a smaller amount of time has been spent on implementing the results of such measurements. Future work could use these measured impedances to update closed loop control systems in real time. To implement these techniques into a final physical device would require careful attention to the abilities of the controller as well as the structure of the overall program. As great quantities of sampled data are being stored locally, large amounts of robust, fast memory would be necessary. The feasibility of such systems should only improve with time as the cost of more capable devices and memory are trending downwards. Also, ongoing developments in the field of Digital Signal Processing have shown the possibility of even more efficient FFT algorithms. [19] Such “sparse” FFT implementations could lessen the requirements of the identification system.

One interesting possibility is the use of machine learning to improve the impedance estimations. The methods used here are admittedly simplistic in their attempts at data fitting to a parametric model. The emerging field of machine learning has shown the possibility of sophisticated data manipulation through the use of flexible learning and

constantly evolving systems. Such a system could possibly recognize and act on patterns not immediately obvious to the programmer.

REFERENCES

- [1] Ming-Tsung, "Analysis and Design of Three-Phase AC-to-DC Converters With High Power Factor and Near-Optimum Feedforward," *IEEE Transactions on Industrial Electronics*, vol. 46, no. 3, pp. 535-543, 1999.
- [2] M. P. Kazmierkowski, "Review of Current Regulation Techniques For Three-Phase PWM Inverters," in *IEEE ISIE*, 1993.
- [3] A. L. Trigo, "A Linear Time Model of The Voltage Source Converter for STATCOM Applications," in *PSCC*, Liege, 2005.
- [4] P. Lehn, "Exact Modeling of the Voltage Source Converter," *IEEE Transactions on Power Delivery*, vol. 17, no. 1, pp. 217-222, 2002.
- [5] D. Martin, "Auto Tuning of Digital Deadbeat Current Controller for Grid Tied Inverters Using Wide Bandwidth Impedance Identification," *IEEE*, pp. 277-284, 2012.
- [6] B. Miao, "System Identification of Power Converters With Digital Control Through Cross-Correlation Methods," *IEEE*, pp. 1093-1099, 2005.
- [7] D. Martin, "Wide Bandwidth System Identification of AC System Impedance by Applying Perturbations to an Existing Converter," *IEEE*, pp. 2549-2556, 2011.
- [8] A. Barkley, "Improved Online Identification of Switching Converters Using Digital Network Analyzer Techniques," in *Power Electronics Specialists Conference, PESC 2008. IEEE*, 2008.
- [9] K. Borisov, "Experimental Investigation of Submarine Drive Model With PWM-Based Attenuation of Acoustic and Electromagnetic Noise," University of Nevada, Reno, 2003.
- [10] K. Borisov, "Attenuation of Electromagnetic Interference in a Shunt Active Power Filter," *IEEE Transactions on Power Electronics*, vol. 22, no. 5, pp. 1912-1918,

2007.

- [11] L. Ljung, System Identification: Theory for the User, Englewood Cliffs: Prentice-Hall, 1987.
- [12] Q. Bi, "Robust Identification of First-order Plus Dead-time Model from Step Response," *Control Engineering Practice* , vol. 7, pp. 71-77, 1999.
- [13] S. Ahmed, "Novel Identification Method from Step Response," *Control Engineering Practice*, vol. 15, pp. 545-556, 2007.
- [14] D. S. Moore, The Basic Practice of Statistics 3rd Edition, New York: W. H. Freeman and Company, 2004.
- [15] R. W. Erickson, Fundamentals of Power Electronics Second Edition, Norwell: Kluwer Academic Publishers, 2001.
- [16] A. Barkley, "Adaptive Control of Power Converters Using Digital Network Analyzer Techniques," University of South Carolina, Columbia .
- [17] D. Martin, "Wide Bandwidth Three-Phase Impedance Identification using Existing Power Electronics Inverter," *IEEE*, pp. 334-341, 2013.
- [18] J. H. McClellan, DSP First, Upper Saddle River: Prentice-Hall, 1999.
- [19] H. Hassaneih, "Simple and Practical Algorithm for Sparse Fourier Transform," in *ACM-SIAM Symposium on Discrete Algorithms*, Kyoto, 2012.

APPENDIX A – RPWMII MATLAB S-FUNCTION

```

function RPWMtwo(block)
setup(block)
%endfunction

%%
% 1 - Get system parameters
% 2 - Enter loop
% 3 - Get system time
% 4 - If system time == n*sample time
%     - Sample inputs
%     - Calculate time delay
%     - If system time == calculated time set pwm
%     - Set sampled outputs
%

%% Function: setup =====
%% Abstract:
%% Inputs
% 1 - Duty Cycle Reference
% 2 - System Time
% 3 - Random Values
%
%% Outputs
% 1 - Sampled input data
% 2 - Generated PWM
% 3 - Generated Frequency
%%
function setup(block)

block.NumInputPorts = 3;
block.NumOutputPorts = 3;

% Setup port properties to be inherited or dynamic
block.SetPreCompInPortInfoToDynamic;
block.SetPreCompOutPortInfoToDynamic;

% Override input port properties
block.InputPort(1).Dimensions = block.DialogPrm(1).Data; %Reference
block.InputPort(1).DatatypeID = 0; % double
block.InputPort(1).Complexity = 'Real';
block.InputPort(1).SamplingMode = 'Sample';
% Override input port properties
block.InputPort(2).Dimensions = 1; %System Time
block.InputPort(2).DatatypeID = 0; % double
block.InputPort(2).Complexity = 'Real';
block.InputPort(2).SamplingMode = 'Sample';

% Override input port properties

```

```

block.InputPort(3).Dimensions = block.DialogPrm(6).Data; %Sample inputs
block.InputPort(3).DatatypeID = 0; % double
block.InputPort(3).Complexity = 'Real';
block.InputPort(3).SamplingMode = 'Sample';

% Override input port properties
block.OutputPort(1).Dimensions = block.DialogPrm(1).Data; %Sampled data
block.OutputPort(1).DatatypeID = 0; % double
block.OutputPort(1).Complexity = 'Real';
block.OutputPort(1).SamplingMode = 'Sample';

% Override input port properties
block.OutputPort(2).Dimensions = block.DialogPrm(6).Data; %Generated PWM
block.OutputPort(2).DatatypeID = 0; % double
block.OutputPort(2).Complexity = 'Real';
block.OutputPort(2).SamplingMode = 'Sample';

% Override input port properties
block.OutputPort(3).Dimensions = block.DialogPrm(6).Data; %Generated Frequency
block.OutputPort(3).DatatypeID = 0; % double
block.OutputPort(3).Complexity = 'Real';
block.OutputPort(3).SamplingMode = 'Sample';

% Register parameters
block.NumDialogPrms = 6;
% 1 - Number of inputs to sample
% 2 - Sample time
% 3 - Simulation time
% 4 - Period
% 5 - Max frequency (input as minimum period)
% 6 - Number of PWM's to generate

% Register sample times
% [0 offset] : Continuous sample time
% [positive_num offset] : Discrete sample time
%
% [-1, 0] : Inherited sample time
% [-2, 0] : Variable sample time
block.SampleTimes = [-1 0];

%block.SimStateCompliance = 'DefaultSimState';

block.RegBlockMethod('PostPropagationSetup', @DoPostPropSetup);
block.RegBlockMethod('InitializeConditions', @InitializeConditions);
block.RegBlockMethod('Start', @Start);
block.RegBlockMethod('Outputs', @Outputs); % Required
block.RegBlockMethod('Update', @Update);
block.RegBlockMethod('Derivatives', @Derivatives);
block.RegBlockMethod('Terminate', @Terminate); % Required
%block.RegBlockMethod('GetSimState', @GetSimState);
%block.RegBlockMethod('SetSimState', @SetSimState);

%end setup

```

```

%%
%% PostPropagationSetup:
%%
function DoPostPropSetup(block)
block.NumDworks = 12;

block.Dwork(1).Name      = 'Duty_Cycle';
block.Dwork(1).Dimensions = 1;
block.Dwork(1).DatatypeID = 0;    % double
block.Dwork(1).Complexity = 'Real'; % real
block.Dwork(1).UsedAsDiscState = true;

block.Dwork(2).Name      = 'System_Time';
block.Dwork(2).Dimensions = 1;
block.Dwork(2).DatatypeID = 0;    % double
block.Dwork(2).Complexity = 'Real'; % real
block.Dwork(2).UsedAsDiscState = true;

block.Dwork(3).Name      = 'Random_Vals';
block.Dwork(3).Dimensions = 1;
block.Dwork(3).DatatypeID = 0;    % double
block.Dwork(3).Complexity = 'Real'; % real
block.Dwork(3).UsedAsDiscState = true;

block.Dwork(4).Name      = 'Output_State';
block.Dwork(4).Dimensions = 1;
block.Dwork(4).DatatypeID = 0;    % double
block.Dwork(4).Complexity = 'Real'; % real
block.Dwork(4).UsedAsDiscState = true;

block.Dwork(5).Name      = 'Start_Time';
block.Dwork(5).Dimensions = 1;
block.Dwork(5).DatatypeID = 0;    % double
block.Dwork(5).Complexity = 'Real'; % real
block.Dwork(5).UsedAsDiscState = true;

block.Dwork(6).Name      = 'Finish_Time';
block.Dwork(6).Dimensions = 1;
block.Dwork(6).DatatypeID = 0;    % double
block.Dwork(6).Complexity = 'Real'; % real
block.Dwork(6).UsedAsDiscState = true;

block.Dwork(7).Name      = 'Period';
block.Dwork(7).Dimensions = 1;
block.Dwork(7).DatatypeID = 0;    % double
block.Dwork(7).Complexity = 'Real'; % real
block.Dwork(7).UsedAsDiscState = true;

block.Dwork(8).Name      = 'Flag';
block.Dwork(8).Dimensions = 1;
block.Dwork(8).DatatypeID = 0;    % double
block.Dwork(8).Complexity = 'Real'; % real
block.Dwork(8).UsedAsDiscState = true;

```

```

block.Dwork(9).Name      = 'Center_Freq';
block.Dwork(9).Dimensions = 1;
block.Dwork(9).DatatypeID = 0;    % double
block.Dwork(9).Complexity = 'Real'; % real
block.Dwork(9).UsedAsDiscState = true;

block.Dwork(10).Name      = 'PWM_time';
block.Dwork(10).Dimensions = 1;
block.Dwork(10).DatatypeID = 0;    % double
block.Dwork(10).Complexity = 'Real'; % real
block.Dwork(10).UsedAsDiscState = true;

block.Dwork(11).Name      = 'temp';
block.Dwork(11).Dimensions = 1;
block.Dwork(11).DatatypeID = 0;    % double
block.Dwork(11).Complexity = 'Real'; % real
block.Dwork(11).UsedAsDiscState = true;

block.Dwork(12).Name      = 'PWM';
block.Dwork(12).Dimensions = 1;
block.Dwork(12).DatatypeID = 0;    % double
block.Dwork(12).Complexity = 'Real'; % real
block.Dwork(12).UsedAsDiscState = true;

%%
%% InitializeConditions:
%%
function InitializeConditions(block)

%end InitializeConditions

%%
%% Start:
%%
function Start(block)
    block.Dwork(1).Data = 0;    % Duty
    block.Dwork(2).Data = 0;    % System time
    block.Dwork(3).Data = 0;    % r1
    block.Dwork(4).Data = 0;    % r2
    block.Dwork(5).Data = 0;    % t1
    block.Dwork(6).Data = 0;    % t2
    block.Dwork(7).Data = block.DialogPrm(4).Data;    % tau
    block.Dwork(8).Data = block.DialogPrm(4).Data;    % tsw
    block.Dwork(9).Data = 0;    % Center Frequency Value
    block.Dwork(10).Data = 0;
    block.Dwork(11).Data = block.DialogPrm(4).Data;
    block.Dwork(3).Data = 0 + (1-0).*rand(1,1);    % Generate r1
    block.Dwork(5).Data = block.Dwork(3).Data * block.Dwork(7).Data;

%endfunction

%%
%% Outputs:

```

```

%%
function Outputs(block)

%%end Outputs

%%
%% Update:
%%
function Update(block)

    %block.Dwork(1).Data = block.InputPort(1).Data; %Read Duty
    %block.Dwork(2).Data = block.InputPort(1).Data; %Read Clock
    %block.Dwork(3).Data = block.InputPort(3).Data; %Read Random
    %block.OutputPort(3).Data = 2/block.Dwork(12).Data; %Display t_switching
    %Peaks are freq

    block.Dwork(2).Data = block.Dwork(2).Data + block.DialogPrm(3).Data; %Create sample time
    if(block.Dwork(2).Data>= block.DialogPrm(2).Data)
        %Sampling
        block.Dwork(2).Data = 0;
        %block.OutputPort(1).Data = block.InputPort(1).Data;
        %RPWM
        block.Dwork(4).Data = 0 + (1-0).*rand(1,1); %Gen R2
        block.Dwork(6).Data = block.Dwork(4).Data * block.Dwork(7).Data; %Gen t2
        block.Dwork(8).Data = block.Dwork(7).Data+block.Dwork(6).Data-block.Dwork(5).Data;
        if(block.Dwork(8).Data>block.DialogPrm(5).Data)
            %Do nothing
        else
            block.Dwork(6).Data = block.Dwork(6).Data+block.DialogPrm(5).Data-block.Dwork(8).Data;
            block.Dwork(8).Data = block.DialogPrm(5).Data;
        end
        block.Dwork(5).Data = block.Dwork(6).Data;
        %block.OutputPort(3).Data = 1/block.Dwork(8).Data;

    end

    block.Dwork(10).Data = block.Dwork(10).Data + block.DialogPrm(3).Data; %Create sample time
    %if(pwm_time >= Tsw)
    %get new Tsw
    %reset
    if(block.Dwork(10).Data >= block.Dwork(11).Data)
        block.OutputPort(3).Data = 1/block.Dwork(10).Data;
        block.Dwork(11).Data = block.Dwork(8).Data;
        block.Dwork(10).Data = 0;
        block.Dwork(12).Data = block.InputPort(3).Data * block.Dwork(11).Data;
    end
    if(block.Dwork(10).Data < block.Dwork(12).Data)
        block.OutputPort(2).Data = 1;
    else
        block.OutputPort(2).Data = 0;
    end
    end
    block.OutputPort(3).Data = 1/block.Dwork(11).Data; %/block.Dwork(11).Data;
%%end Update.

```



```
%%  
%% Derivatives:  
%%  
function Derivatives(block)  
  
%end Derivatives  
  
%%  
%% Terminate:  
%%  
function Terminate(block)  
clc;  
%end Terminate
```

APPENDIX B – FFT AVERAGING MATLAB FUNCTION

```
function y = average(array,samples,offset,bits,width)
    x=0;
    offset2=0;
    while(x<=samples)
        %Offset for taking several samples
        %offset = width*x;
        %Cut into smaller pieces of data
        array2 = array(offset2+1:width+offset2);

        %Correct for current sensor gain
        offset2 = offset2+offset;
        %current2 = current2-2.525;
        %current2 = current2/0.5628;

        window = hann(length(array2));
        window = 1;
        FII = fft(array2.*window,bits);      %fft of current * window

    Z=FII;
    switch(x)
        case 0
            Z0=abs(Z);
        case 1
            Z1=abs(Z);
        case 2
            Z2=abs(Z);
        case 3
            Z3=abs(Z);
        case 4
            Z4=abs(Z);
        case 5
            Z5=abs(Z);
        case 6
            Z6=abs(Z);
        case 7
            Z7=abs(Z);
        case 8
            Z8=abs(Z);
        case 9
            Z9=abs(Z);
        case 10
            Z10=abs(Z);
        case 11
            Z11=abs(Z);
        case 12
            Z12=abs(Z);
```

```

        case 13
            Z13=abs(Z);
        case 14
            Z14=abs(Z);
        case 15
            Z15=abs(Z);
        otherwise
            display('Out of bounds');
    end
    x = x + 1;
end

x=1;
while(x<=length(Z1))          %Create the sampled data
    switch(samples)
        case 0
            averaged(x,1)=( Z0(x,1) )./(samples+1);
        case 1
            averaged(x,1)=( Z0(x,1)+Z1(x,1) )./(samples+1);
        case 2
            averaged(x,1)=( Z0(x,1)+Z1(x,1)+Z2(x,1) )./(samples+1);
        case 3
            averaged(x,1)=( Z0(x,1)+Z1(x,1)+Z2(x,1)+Z3(x,1) )./(samples+1);
        case 4
            averaged(x,1)=( Z0(x,1)+Z1(x,1)+Z2(x,1)+Z3(x,1)+Z4(x,1) )./(samples+1);
        case 5
            averaged(x,1)=( Z0(x,1)+Z1(x,1)+Z2(x,1)+Z3(x,1)+Z4(x,1)+Z5(x,1) )./(samples+1);
        case 6
            averaged(x,1)=( Z0(x,1)+Z1(x,1)+Z2(x,1)+Z3(x,1)+Z4(x,1)+Z5(x,1)+Z6(x,1) )./(samples+1);
        case 7
            averaged(x,1)=( Z0(x,1)+Z1(x,1)+Z2(x,1)+Z3(x,1)+Z4(x,1)+Z5(x,1)+Z6(x,1)+Z7(x,1)
            )./(samples+1);
        case 8
            averaged(x,1)=( Z0(x,1)+Z1(x,1)+Z2(x,1)+Z3(x,1)+Z4(x,1)+Z5(x,1)+Z6(x,1)+Z7(x,1)+Z8(x,1)
            )./(samples+1);
        case 9
            averaged(x,1)=(
            Z0(x,1)+Z1(x,1)+Z2(x,1)+Z3(x,1)+Z4(x,1)+Z5(x,1)+Z6(x,1)+Z7(x,1)+Z8(x,1)+Z9(x,1) )./(samples+1);
        case 10
            averaged(x,1)=(
            Z0(x,1)+Z1(x,1)+Z2(x,1)+Z3(x,1)+Z4(x,1)+Z5(x,1)+Z6(x,1)+Z7(x,1)+Z8(x,1)+Z9(x,1)+Z10(x,1)
            )./(samples+1);
        case 11
            averaged(x,1)=(
            Z0(x,1)+Z1(x,1)+Z2(x,1)+Z3(x,1)+Z4(x,1)+Z5(x,1)+Z6(x,1)+Z7(x,1)+Z8(x,1)+Z9(x,1)+Z10(x,1)+Z11(x,1)
            )./(samples+1);
        case 12
            averaged(x,1)=(
            Z0(x,1)+Z1(x,1)+Z2(x,1)+Z3(x,1)+Z4(x,1)+Z5(x,1)+Z6(x,1)+Z7(x,1)+Z8(x,1)+Z9(x,1)+Z10(x,1)+Z11(x,1)
            +Z12(x,1) )./(samples+1);
        case 13
            averaged(x,1)=(
            Z0(x,1)+Z1(x,1)+Z2(x,1)+Z3(x,1)+Z4(x,1)+Z5(x,1)+Z6(x,1)+Z7(x,1)+Z8(x,1)+Z9(x,1)+Z10(x,1)+Z11(x,1)
            +Z12(x,1)+Z13(x,1) )./(samples+1);
        case 14

```

```

        averaged(x,1)=(
Z0(x,1)+Z1(x,1)+Z2(x,1)+Z3(x,1)+Z4(x,1)+Z5(x,1)+Z6(x,1)+Z7(x,1)+Z8(x,1)+Z9(x,1)+Z10(x,1)+Z11(x,1
)+Z12(x,1)+Z13(x,1)+Z14(x,1) )./(samples+1);
        case 15
            averaged(x,1)=(
Z0(x,1)+Z1(x,1)+Z2(x,1)+Z3(x,1)+Z4(x,1)+Z5(x,1)+Z6(x,1)+Z7(x,1)+Z8(x,1)+Z9(x,1)+Z10(x,1)+Z11(x,1
)+Z12(x,1)+Z13(x,1)+Z14(x,1)+Z15(x,1) )./(samples+1);
            otherwise
                display('Out of bounds');
            end

        %averaged_phase(x,1)= atan(imag(averaged(x,1))./real(averaged(x,1)))*180/pi;
        x = x + 1;
    end
    y = averaged;

```

APPENDIX C – LEAST SQUARES MATLAB FUNCTION

```
function y = leastSquares(array) %Array(x,1)=freq Array(x,2)=magnitude
sum_X=0;
sum_Y=0;
sum_XX = 0;
sum_XY = 0;
output = 0;
n=length(array);
x=1;
while(x<=length(array))
    sum_X = array(x,1) + sum_X;
    sum_Y = (array(x,2)) + sum_Y;
    sum_XX = (array(x,1)*array(x,1)) + sum_XX;
    sum_XY = (array(x,1)*(array(x,2))) + sum_XY;
    x=x+1;
end

den = n*sum_XX - (sum_X)^2;
slopenum = n*sum_XY - sum_X*sum_Y;
bnum = sum_Y*sum_XX - sum_X*sum_XY;

slope=slopenum./den;
intercept=bnum./den;

x=1;
while(x<=length(array))
    output(x,1)=array(x,1);
    output(x,2)=(array(x,1).*slope+intercept);
    x=x+1;
end

y = output;
```